Hot Electron Resistance and Magnetoresistance in High Purity Gallium Arsenide

by
Eric Sven Hellman

A DISSERTATION
SUBMITTED TO THE DEPARTMENT OF ELECTRICAL ENGINEERING
AND THE COMMITTEE ON GRADUATE STUDIES
OF STANFORD UNIVERSITY
IN PARTIAL FULFILLMENT OF THE REQUIREMENTS
FOR THE DEGREE OF
DOCTOR OF PHILOSOPHY

May 1987

I certify that I have read this thesis and that in my opinion it is fully adequate, in scope and quality, as a dissertation for the degree of Doctor of Philosophy.

_____

(Principal Advisor)

I certify that I have read this thesis and that in my opinion it is fully adequate, in scope and quality, as a dissertation for the degree of Doctor of Philosophy.

_____

I certify that I have read this thesis and that in my opinion it is fully adequate, in scope and quality, as a dissertation for the degree of Doctor of Philosophy.

_____

Approved for the University Committee on Graduate Studies:

_____

Dean of Graduate Studies

Abstract

Electrons in strong magnetic fields are confined to one dimension and can have properties not found in three dimensional electron systems. This dissertation will describe theoretical investigations into the mechanisms of phonon emission by electrons confined to one dimension. It will then review previous work on the role of phonon emission in GaAs/$Al_xGa_{1-x}As$ heterojunction tunneling experiments which have indicated that the transport of energetic electrons in very lightly doped GaAs has an unusual behavior when strong magnetic fields are applied parallel to the direction of current flow. It will also report on experimental measurements of the high electric field resistivity of bulk GaAs parallel to strong magnetic fields. For these experiments, very lightly silicon doped GaAs was grown on semi-insulating substrates by molecular beam epitaxy in a chamber demonstrated to produce very high purity material. The current-voltage curves of small resistors made from this material reveal a variety of phenomena, including carrier heating, donor freeze-out, magnetic freeze-out, and impact ionization. At liquid helium temperature, the magnetic field sweeps reveal resonant ionization phenomena. At liquid nitrogen temperatures, the magnetic fields appear to enhance the electron cooling and suppress phenomena related to valley transfer of electrons. These bulk measurements, together with data from heterostructure tunneling experiments, provide new understanding of the interactions between electrons, phonons and impurities in GaAs at low temperatures.

Other Work

A large part of my time at Stanford has been spent working on topics which are only related peripherally to the study of electron magneto-transport in GaAs. This work is summarized in Appendix 3.

Acknowledgments

The magical part of doing graduate work is working with, and learning from, other people. My thesis advisor, "Coach" Jim Harris, has taught me a great deal about how to do science, and other things, too. I have been amazed at his continual enthusiasm and encouragement, even when I would discuss obscure phenomena with him at 2AM. As the cliché goes, without Prof. Harris, this work would not have been possible. But the lab wouldn't have existed either. The lab might have existed, but it would have been poorer but for the efforts of several other students, especially Phil Pitner.

Many, many people helped me out with the work described in this dissertation. During the theoretical work on polarons, I profited greatly by working with Prof. Bob Laughlin and Charles Hanna. I most appreciate Prof. Laughlin's advice and keen skepticism. Conversations with Tom Hickmott and Prof. Lawrence Eaves greatly influenced my thinking about the heterojunction tunneling experiments. The experimental work was very dependent on help from other people. The high purity MBE work was driven by the enthusiasm of Eric Larkins. The resistor fabrication process was derived from the work of Alex Harwit and Paul Delahoussaye, and wouldn't have fabricated anything without their help. Other people who helped out in this area were Won-Seong Lee, Kanji Yoh, Darrell Schlom, Byung-Gook Park and Mark Rodwell. The low temperature, high magnetic field measurements were all done in a system belonging to Prof. Aharon Kapitulnik, and I appreciate the assistance of Charles Hanna and Kookrin Char. Many others helped out in small but indispensable ways.

The manuscript has benefitted from the criticisms and corrections of Karen Liu and my reading committee: Profs. Harris, Swanson and Villard. Any spelling misteaks are entirely the fault of Microsoft Corporation.

I am happy to acknowledge fellowship support during my tenure at Stanford from the National Science Foundation and from IBM Corporation. The research described in the dissertation was supported by the Joint Services Electronics Program and by the Defense Advanced Research Projects Agency.

Dedication

To K. Liu, who liked my “theory” vest.

Table of Contents

List of Figures

1. Introduction

Modern technology has made possible the study of very small devices and artificially structured materials. In these systems, physical phenomena can have quantum coherence lengths comparable to the size of the structures, even at room temperature. For example, using molecular beam epitaxy (MBE) or metallorganic chemical vapor deposition (MOCVD), high purity layered crystalline semiconductors can be grown with atomic layer by atomic layer control. These layered structures retain perfect translational symmetry in two of three spatial dimensions, and carriers can be confined by crystal potentials in the third dimension. The combination of the small length scale of the layering and small scattering by imperfections results in large quantum effects. In recent years, investigations into the physics of electrons in these two dimensional semiconductor structures have uncovered a wealth of new phenomena, in large part due to the availability of "clean" systems. The combination of atomically smooth surfaces and confinement of electrons to two dimensions has allowed the discovery of the quantum Hall effect[1] and the fractional quantum Hall effect.[2] Already, the high mobility made possible by modulation doped heterostructures,[3] in which the donor atoms are physically separated from the carriers they donate, is being applied to high density electronic circuits.[4]

Electrons confined to one dimension have so far been much more difficult to realize experimentally, due to the extreme difficulty of fabricating lateral structures on an atomic scale. Nonetheless, progress in this area has been extremely rapid. Initial experiments on one dimensional electron systems concentrated on very narrow metal wires formed by shadow evaporation, and on organic chain polymers whose structures are intrinsically one dimensional. More recently, high resolution electron beam lithography has been used to carve narrow lines from silicon MOSFET's.[5,6] New phenomena observed in these semiconductor structures include "telegraph" (discrete level switching) signals from single electron traps[7] and the so-called "universal conductance fluctuations".[8] These wires are "dirty" systems. The phenomena observed in the very narrow MOSFET's are due to *strong* scattering of the electron waves, in contrast to the quantum Hall

effect in the 2-dimensional modulation-doped structures, which is destroyed by strong scattering and is only seen in "clean" systems. Exotic methods for making "clean" one- (and zero-) dimensional semiconductor "wires" (and "dots") have been proposed by several workers.[9] However, the most successful attempts at fabrication have so far involved simple etching of tiny patterns into layered crystals, or using ion-implantation to isolate very small areas. Reed[10], Petroff[11] and Kash[12] have observed photo-luminescence in such quantum dots and wires of GaAs showing lateral size-effect energy shifts. They also observe luminescence efficiency significantly higher than observed for bulk material, which is surprising because of the close proximity of un-passivated surfaces to the carriers in these structures. It is unclear whether this is a strictly dimensional effect or related to defects, but the promise of new and interesting results is clear.

Another way to study electrons confined to one dimension is to study electrons in strong magnetic fields. Classical electrons follow orbits which spiral around the magnetic field lines. When the radius of the spiral is comparable to the wavelength of the electron, the electron's motion perpendicular to the field is quantized, and it becomes effectively one dimensional.[a] The wavefunctions for free electrons in a magnetic field $\mathbf{H}=H\hat{z}$, using the Landau gauge for the vector potential are:[13]

$$|k_x,k_z,m\rangle = \frac{1}{\Omega^{1/3}C_m} e^{ik_x x+ik_z z} e^{-Y^2/2} H_m(Y) \qquad (1)$$

where Ω is the system volume, the $H_m(x)$ are the Hermite polynomials, the normalization factors are $C_m=(2^m m!\sqrt{\pi}L)^{-1/2}$, the center of the wavefunction in the $\hat{y}$ direction is at

$$Y = \frac{y-k_X L^2}{L} \qquad (2)$$

and the magnetic confinement length is

[a] Although the electrons in a magnetic field have two momentum eigenvalues, the kinetic energy depends only on the momentum parallel to the magnetic field. The energy density of states is thus one-dimensional.

$$L = \sqrt{\frac{\hbar c}{eH}} \quad . \tag{3}$$

These are energy eigenstates of the electron Hamiltonian with eigenvalues

$$E_{k_x,k_z,m} = \frac{\hbar^2 k_z^2}{2} + (m+1/2)\hbar\omega_c \tag{4}$$

where

$$\hbar\omega_c = \frac{eH}{m^* c} \tag{5}$$

is the cyclotron energy. Since the states are degenerate with respect to k_x the electrons are effectively one dimensional when $\hbar\omega_c$ is large. They are not truly one-dimensional, because electric fields perpendicular to the magnetic field introduce Lorentz forces which push the electrons perpendicular to both the electric and magnetic fields and break the k_x degeneracy. However, electric fields parallel to the magnetic field do not change the one dimensional character of the confined electrons. Thus, strong magnetic fields offer a unique (and inexpensive) way to study the behavior of one dimensional electrons without the strong scattering present in the real heterostructures of today.

In this dissertation, I will report on theoretical and experimental studies into the physics of electrons confined by strong magnetic fields. I will concentrate on the transport of such electrons when they are accelerated by electric fields parallel to the confining magnetic fields. These electrons become considerably more energetic than thermally excited electrons and are thus considered to be “hot” (or maybe “warm”, as will be discussed in Section 4.5). In polar semiconductors such as GaAs, these hot electrons exchange energy with the crystal lattice primarily by emitting longitudinal optical phonons. These phonons interact strongly with the electrons because the adjacent atoms vibrate out of phase with each other. In polar materials, the adjacent atoms are oppositely charged, and the atomic dipoles caused by

the lattice vibrations build up electric fields which are felt directly by the electrons.

Phonons are virtually unaffected by the magnetic fields which confine electrons. (Although confined phonon modes can exist in compositional heterostructures, I will not consider these effects at all. Phonons are generally not confined in the very common x=0.3 $Al_xGa_{1-x}As/GaAs$ heterostructures.) The effect of confinement on the interactions of electrons and phonons comes primarily through changes in the density of electron states. Figure 1 shows the electron energy dependence of the density per unit energy of electron states, with the dimension as a parameter. In three dimensions, the density of states is proportional to the square root of the electron energy. The surface area of constant energy spheres increases as the square of the radius in three dimensions; the increasing density of states follows. In one dimension, the surface "area" of a "sphere" is *independent* of "radius".(A line has two ends independent of its length.) The density of states then works out to be proportional to the *inverse* square root of the energy. This means that there is a divergence at zero energy. Scattering rates are generally proportional to the density of available final states. For elastic scattering, in which the electrons do not change energy, the density of final states may be much smaller in one dimension compared to three. For this reason, Sakaki[14] has argued that the mobility of electrons confined to one dimension would be strongly enhanced. For scattering by optical phonons, however, the situation may be quite different. Since optical phonon emission or absorption is an inelastic process, electrons of the right energy can scatter to zero energy states, where the number of available final states is very large in one dimension. This is depicted in figure 2. An electron with exactly the energy of a phonon is scattered to the bottom of the parabolic band, where the energy density of states actually diverges for ideal one dimensional electrons. The result of this divergence is that electrons of the appropriate energy interact very strongly with phonons.

What happens when an electron has exactly the right energy to emit a phonon? Can the effects of the divergence of the electron density of states be seen in transport measurements? These are the questions that led to the work described in this thesis. In Chapter 2, I will present a theoretical treatment of phonon emission and the electron phonon interaction in one dimensional systems. In Chapter 3, I will review recent experimental work on the

appearance of phonon structure in the current-voltage characteristics of semiconductor tunnel barriers when quantizing magnetic fields are applied, and I will examine the possibility that the one-dimensional effects predicted in Chapter 2 play a role in these experiments. In Chapter 4, I will present the results of a set of experiments designed to look for the effects of Chapter 2 in bulk transport measurements. Finally, I will discuss the interrelations of the experiments of Chapters 3 and 4, and will suggest further ways to look for the one-dimensional effects of Chapter 2.

Figure 1. Dependence of the energy density of states on electron energy, for one, two and three dimensional electrons in parabolic bands.

Figure 2. Elastic and inelastic scattering processes differ in one dimension because inelastic scattering can take have an infinite density of final states.

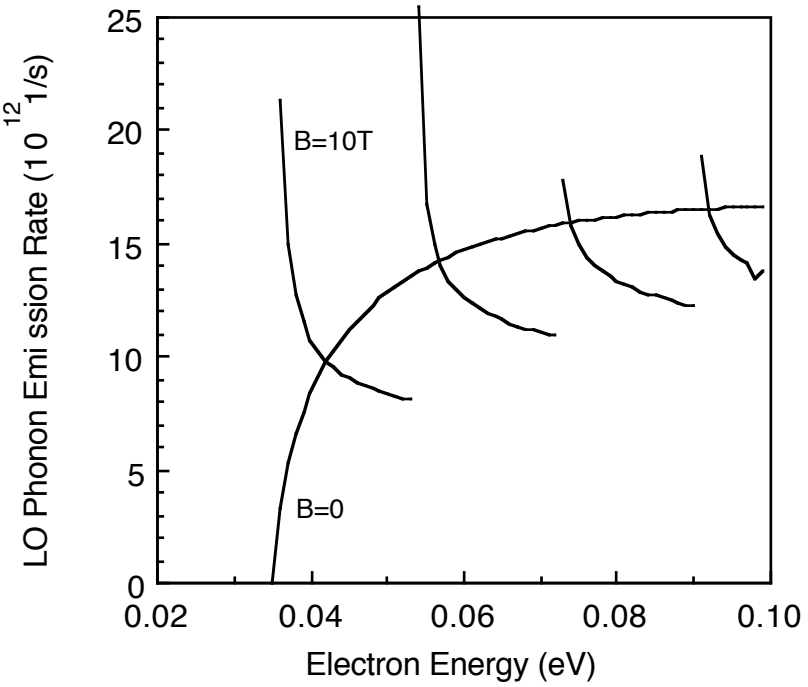

Figure 3. Dependence of emission rate of longitudinal optical phonons by electrons in GaAs on electron energy and magnetic field. Emission rate is calculated using Fermis Golden Rule. Each of the gray curves, which give the emission rate in a magnetic field of 10T, go to infinity for energies such that the final energy lies at the bottom of a magnetic sub-band. The electrons are assumed to be initially in the lowest Landau level.

2. Phonon Emission and Polarons in One Dimension

The interaction of electrons with polar optical phonons is of interest for both practical and fundamental reasons. The range of materials in which the polar electron-phonon interaction dominates electron transport extends from the semiconducting III-V compounds to the insulating alkali-halides, and even includes glasses such as SiO_2 and surfaces of liquid helium. On the other hand, polarons, which are the quasiparticles associated with the interacting electron-phonon system, were the result of the first application of quantum field theoretical methods to condensed matter physics.[15] Recent work on the electron-phonon interaction has emphasized the effects of reduced dimensionality on polarons and electron-phonon scattering.[16]

The standard treatment of electron-phonon scattering processes such as phonon emission involves the use of perturbation theory. Longitudinal optical (LO) phonons, which have energy $\hbar\omega_{LO}$, can be emitted by electrons with energy greater than $\hbar\omega_{LO}$. To calculate the rate of phonon emission, Fermi's golden rule is used. Fermi's golden rule is derived by treating the interaction of electrons and phonons as a small perturbation to the non-interacting electron and phonon Hamiltonian, and discarding terms higher than first order in the small perturbation to get:

$$\text{rate} = (2\pi/\hbar) \sum_{f} |\langle i|H_{e\text{-}\varphi}| f\rangle|^2 \quad . \tag{6}$$

The sum over final states implies that for a given initial energy E, the phonon emission rate is proportional to the density of free electron states at energy $E-\hbar\omega_{LO}$. Using Fermi's golden rule, it is straightforward to calculate the phonon emission rate for an electron of energy E. The electron-phonon interaction is usually described by the Hamiltonian given by Fröhlich[15]:

$$H_{e\text{-}\varphi} = \sum_{\mathbf{q}} V_q \, e^{-i\mathbf{q}\cdot\mathbf{r}} \, (a^{\dagger}_{\mathbf{q}} + a_{-\mathbf{q}}) \tag{7}$$

where

$$V_q = \hbar\omega_{LO}\sqrt{\frac{4\pi\alpha}{\Omega\, k_{LO}}}\ \frac{1}{q} \tag{8}$$

and α is the dimensionless coupling constant:

$$\alpha = \frac{m^* e^2}{\hbar^2 k_{LO}(\varepsilon_\infty^{-1} - \varepsilon_0^{-1})^{-1}} \tag{9}$$

and $k_{LO}=\sqrt{2m^*\omega_{LO}/\hbar}$ is the wave vector of an electron with energy $\hbar\omega_{LO}$. In this expression, the electron is treated using the notation of first quantization, while the phonons are in second quantization. In other words, the electrons, with wave vectors **r**, have the familiar plane wave wave-functions, while the phonons, with wave vectors **q**, have the creation and destruction operators $a^\dagger_{\mathbf{q}}$ and $a_{\mathbf{q}}$, which represent the creation and destruction of phonons. These operators satisfy the commutation relations $[a^\dagger_{\mathbf{q}}, a_{\mathbf{q}'}]=\delta_{\mathbf{q},\mathbf{q}'}$, which automatically give the Bose statistics to the phonons. The matrix element V_q contains the strength of the interaction, and its dependence on the phonon wave vector[b] . The coupling constant α depends on the material. In GaAs, $\alpha \approx .07$[17] which indicates that the perturbation is indeed weak and can be treated using perturbation theory. In very polar materials (e.g. rock salt) $\alpha \geq 1$ and the usual perturbative calculation techniques cannot be used.

The result of a calculation of the phonon emission rate for three dimensional electrons in GaAs using Fermi's golden rule is shown as the solid curve in figure 3. Below $\hbar\omega_{LO}$ no phonons can be emitted. Above $\hbar\omega_{LO}$ the emission rate increases with energy, roughly proportional to the square root of $E-\hbar\omega_{LO}$, due to the increasing number of available final states. At energies well above $\hbar\omega_{LO}$ the emission rate begins to drop due to the 1/q dependence of V_q. For electrons confined to two dimensions, a similar calculation leads to a steplike dependence of the scattering rate on electron energy.[18] Figure 3 also shows the calculated emission rate for an electron in a magnetic field of 10 tesla as the grey curve. At this field the radius of the

[b] **Bold face** will be used for vectors and normal type for scalars, so $q = |\mathbf{q}|$.

classical electron orbit is only 81Å, giving a one dimensional quantization energy of 17meV in GaAs. An electron confined to one dimension has an energy density of states which is proportional to $E^{-1/2}$ and thus diverges at zero energy. As a consequence, the phonon emission rate diverges for electrons with kinetic energy equal to the phonon energy[19], or with energy one phonon above the bottom of one of the magnetic sub-bands (Landau levels). Although this divergence is not disastrous, it should be a hint that something interesting may happen.

In addition to phonon emission and absorption, the electron-phonon interaction can change the effective mass and propagation velocity of the electrons themselves. These properties are given by the electron's dispersion, or energy-momentum, relation. The energy shifts of the electron states induced by the electron-phonon interaction can be calculated using perturbation theory. This is done by keeping terms to 2nd order in the perturbation, resulting in the standard formula

$$\Delta E_i = \sum_f \frac{|\bullet i|H_{e\text{-}\varphi}| f®|^2}{(E_i - E_f)} \quad . \qquad (10)$$

For the unshifted state at k_{LO} ,the number of states for which the denominator of this expression is close to zero gets very large in one dimension. Thus the energy shift becomes very large (it diverges), making the energy negative.[20] This is not possible physically, and indicates that the first order treatment of this problem fails to properly describe the behavior of one dimensional electrons near the phonon emission threshold. Figure 4 shows the behavior of the energy-momentum relation of the combined electron-phonon system in the presence of the electron phonon interaction. The solid curves give the energy momentum relation with the interaction turned off. For energies below the phonon energy, there can be no phonons in the system, and the electron must take up all the momentum. Above the phonon energy, a phonon can exist, and since the energy of an optical phonon is roughly independent of its momentum, the momentum of the electron is no longer specified. Thus, there is a continuum of one-phonon states above the phonon energy. When the interaction is turned on, the zero-

phonon and one-phonon states can mix in ways that allow the interaction to lower the total energy of the state.

To understand the behavior of one dimensional electrons near the phonon emission threshold, I calculated the energy-momentum relation for the coupled electron phonon system using a technique which did not depend on the strength of the interaction. I chose to use the Variational Method, in which one chooses a parametrized wavefunction, calculates the energy, and then varies the parameters so as to minimize the energy. The Variational Principle then tells us that the energy of the correct state must be lower than the minimized energy. The trick to doing an accurate variational calculation is to construct the trial wavefunction in a clever way. A detailed description of the variational calculation is given in Appendix I. The basic assumptions and approximations are as follows:

- Since I'm interested in one-dimensional electrons, I consider the large magnetic field limit. If the magnetic field is large enough to make the cyclotron energy larger than the energy shifts due to the interaction, an accurate calculation can use a trial wavefunction which includes only the contributions of the first Landau level.
- A Fröhlich Hamiltonian is used the calculate the interaction between electrons and phonons. The phonon energy is thus assumed to be independent of its momentum.The Hamiltonian of (7) must be modified slightly to take into account the fact that the electron states in a magnetic field are no longer plane waves. This involves computing matrix elements of the phonon plane waves between the Landau wavefunctions for the electron states. (The Landau gauge for the magnetic vector potential is easiest to use for this purpose.)
- The effects of finite temperature and other broadening are ignored. Thermal phonons are also ignored. Since the Debye temperature is 145°C this assumption is certainly good at liquid nitrogen temperatures and below.
- The trial wavefunction includes contributions from states with two independent phonons. It is relatively easy to include one phonon, and a variational calculation using one phonon results in the same expression as does "Wigner-Brillouin perturbation theory"[21]. The Wigner-Brillouin expression substitutes $E_i - \Delta E_i$ for E_i in equation (10). It works extremely

well for calculating the energy shift at k=0 because there simply isn't enough energy to allow states with more than one phonon to contribute. At the phonon emission threshold, however, the contribution of 2-phonon states to the energy shift is as strong as the contribution of one phonon states to the energy shift at k=0. Figure 4 shows why this is a problem. The energy-momentum curve calculated by Wigner-Brillouin perturbation theory (one of the dotted curves) bends over and "pins" at the phonon energy. However, this is more than one phonon energy above the k=0 energy which has also shifted down due to the interaction. Thus a k=0 polaron (which is a k=0 electron with a cloud of one-phonon, one electron states around it) plus a phonon have less energy than the "pinned" polaron (which, in the same language, is a large wave vector electron with a cloud of one-phonon, one k=0 electron states around it). If 2-phonon states were allowed to contribute, a pinned polaron would consist of a large wave vector electron with a cloud of one-phonon plus k=0 *polaron* states. The two phonon calculation should thus predict that the energy momentum curve pins at one phonon energy above the shifted k=0 energy. This is indeed what happens, as indicated by the curve labeled "this variational calculation" in figure 4.

Although the calculation is done for the case of a large magnetic field, it is easy to see that it has a very close analog in real one dimensional structures. Consider the potential

$$V(\mathbf{r}) = \frac{\hbar^2}{m^* L^4}\,(x^2+y^2) \qquad (11)$$

where L is a characteristic confinement length. This parabolic potential is actually what is expected in many realizations of one dimensional confinement. Using this potential in the Schrödinger equation results in the eigenstates

$$|\, n_x, n_y, k_z\rangle = \frac{C_{n_x} C_{n_y}}{\sqrt{L_z}}\, e^{ik_z z} e^{-(x^2+y^2)/2L^2}\, H_{n_x}(x/L) H_{n_y}(y/L) \qquad (12)$$

where the H_n's are again Hermite polynomials, and

$$C_n=(2^n n!\sqrt{\pi}L)^{-1/2} \tag{13}$$

are normalization constants. $E_0 = \frac{\hbar^2}{m^*L^2}$ is the energy spacing between the sub-bands. Notice the close similarity between these wavefunctions and the magnetic field wavefunctions in given in equation (1). (The confinement length L has been chosen to emphasize the similarity.) It turns out that the electron-phonon interaction Hamiltonian expressed in terms of these electron wave functions is almost identical for magnetically confined electrons and electrons confined by the one-dimensional parabolic potential. (See Appendix 1)

The result of the calculation is shown in figure 5 for the region just below the phonon energy. The calculated energy above the interacting ground state of the polaron is plotted versus the polaron wavevector. The bend-over and pinning of the energy-momentum curves is easily seen. The effect of magnetic field strength is also clear. For larger magnetic fields, the energy separation between the zero-phonon curve and the one-phonon continuum increases. This is because larger magnetic fields increase the density of states in each Landau level, and thus the number of electron states which contribute to the energy lowering is also increased.

A polaron in the pinned region of the curve is a rather unusual particle. Its effective mass, defined as

$$m^* \equiv \hbar^2 \left(\frac{\partial^2 E}{\partial k^2}\right)^{-1} \tag{14}$$

is negative, so that it slows down when "accelerated". The group velocity (the velocity of propagation) is

$$v = \frac{1}{\hbar}\frac{\partial E}{\partial k}. \tag{15}$$

Figure 6 shows a plot of the velocity as a function of wavevector. Notice that the group velocity for the polarons in the pinned region is much smaller than

the velocities in the normal region. The wavefunctions for the pinned polarons consist mostly of states with one phonon carrying most of the momentum and a small momentum electron. These states are bound by the electron-phonon interaction to a zero phonon state with an electron carrying all the momentum. The binding energy holding this particle together is given by the energy separating the polaron curve from the one-phonon continuum. At large wavevectors, this polaron "gap" goes to zero.

The pinning behavior of the energy momentum curve for polarons has been known theoretically for some time.It was predicted by Whitfield and Puff[22] and by Larsen[20] for polarons in three dimensional materials with strong electron-phonon coupling ($\alpha>1$). Even for these strong coupling materials, the pinning results only in a cusp in the energy-momentum relation at the phonon energy. (The polaron gap goes to zero at finite wavevector). Very recently, Peeters et. al.[23] have shown that the pinning behavior is much stronger for polarons confined to two dimensions. The strength of the pinning in strong magnetic fields was hinted at by the work of Larsen[24] but the energy-momentum relation has not been calculated before the present work. Despite this extensive theoretical work, physical effects of the polaron energy-momentum pinning have not been observed experimentally. A similar polaron pinning of Landau levels has been observed as shifts in cyclotron resonance lines.[17] In this experiment, the energy of the second Landau level is observed to pin (as a function of magnetic field) at one phonon energy above the first Landau level. Do pinned polarons really exist?

There are several ways that the polaron pinning might be observed experimentally. First of all, the low velocity of pinned polarons could be observed in time resolved transport experiments. The low velocity could also result in space charge pile-up in structures with narrowly specified electron energy distributions. The density of states at the phonon energy will also be strongly enhanced. (The one dimensional density of states is inversely proportional to the group velocity.) This may be observable in tunneling experiments. The existence of the polaron gap may also manifest itself as a change in the phonon emission rate in strong parallel electric fields. A polaron being accelerated by an electric field should behave like a normal electron until it gets up to the negative effective mass region. Then it should slow down, actually coming to a stop. The electric field should continue to

increase the polaron's momentum until the polaron gap becomes smaller than the natural broadening in the system. At this point emission of a real phonon, unbound to any electrons, should occur. Since optical phonons have finite lifetimes, the phonon lifetime broadening is one possible way for phonons to be emitted across the polaron gap. In GaAs, the optical phonon lifetime is less than 10ps[25], which results in a lifetime broadening of 0.1meV. In large electric fields, broadening due to field emission must also be considered. This can be estimated by calculating the voltage drop across the "size" of the polaron. There is a difference, however, in the process of phonon emission across a gap, and the usual phonon emission process described by Fermi's Golden Rule. The pinned polaron does not gain any energy until it crosses the gap to emit a phonon. In the absence of a gap, an electron continues to gain energy from the electric field. Even in a large electric field, where the gap may not be able to appreciably slow the polaron, the gap will have the effect of increasing the phonon emission probability with respect to the probability that the electron would continue to propagate without emitting a phonon. The result will be that a polaron gap will enhance phonon emission. This effect could show up in transport measurements which are sensitive to the energy distribution of electrons. If a polaron gap exists, the cooling of electrons by phonon emission may be enhanced.

The next two chapters examine experiments in which the existence of polaron pinning might be observed. The first is an experiment revealing the magnetic field dependence of tunneling in GaAs/$Al_xGa_{1-x}As$ hetero-junctions which was done a few years ago by Hickmott and co-workers[26] at the IBM Research Center in Yorktown Heights. The second is an experiment which I have done to search for the effects of a polaron gap.

Figure 4. Schematic energy-momentum relation for the interacting single electron-phonon (polaron) system obtained from second order perturbation theory, Wigner-Brillouin perturbation theory, and the present theory. According to the argument of Whitfield and Puff, the correct curve should bend over at the shifted phonon energy. The ground state energy shift is exaggerated for clarity.

Figure 5. Calculated energy-momentum relation for polarons near the phonon emission threshold for three values of the magnetic field. Energy is with respect to the interacting ground state energy.

Figure 6. Calculated group velocity along the magnetic field for polarons as a function of the wave vector for three magnetic fields. Above k_{LO}, the velocity drops sharply.

3. Phonon Structure in Heterojunction Tunneling Experiments

3.1 Experiments

Tunneling in GaAs/$Al_xGa_{1-x}As$ heterostructures has become of great practical importance for several reasons. Resonant tunneling in double-barrier structures has been observed to occur at very high frequencies,[27] which has raised hopes that such phenomena may form the basis for future high speed electronic circuits. Although the resonant tunneling mechanism has been recognized for decades,[28] fundamental questions concerning the mechanisms of tunneling in heterostructures remain.[29] Tunneling through single barriers is also of great technological importance, due to the use of these barriers in heterojunction field effect transistors (HFET's) and some varieties of hot electron transistors.[30,31] One variety of HFET, the SISFET[c] (semiconductor-insulator-semiconductor field effect transistor)[32,33,34] is a very close analog to the silicon MOSFET (metal-oxide-semiconductor field effect transistor) which is used by the millions in integrated circuits. In the SISFET, heavily doped n-type GaAs is used as the gate "metal", undoped $Al_xGa_{1-x}As$ is used as an insulator, and very lightly doped GaAs is used as the semiconductor. Highly conducting inversion and accumulation layers can be induced at the semiconductor-insulator interface by application of appropriate gate voltage. The nearly ideal interface between GaAs and $Al_xGa_{1-x}As$ makes this a very attractive possibility for high speed GaAs circuits.

T. Hickmott and co-workers at IBM Research Labs in Yorktown, NY were one of several groups who applied their expertise in the MOSFET structures to study the properties of the GaAs/$Al_xGa_{1-x}As$ SISFET structures.[35] The capacitance-voltage (C-V) and current-voltage (I-V) characteristics of these devices could be analyzed using the same techniques used for Si/SiO_2 capacitors to determine doping, insulator fixed charge, and barrier height. However, when they cooled the structures to helium temperatures to study the tunneling properties of thin (200Å) barriers, new

[c] Also known as HIGFET (heterostructure insulating gate FET).

phenomena appeared.[26] In magnetic fields greater than 5T, periodic structure was observed in the current-voltage curves. Current voltage curves measured by Hickmott et. al. are shown in figure 7. The period of the structure, 36 mV, matches the optical phonon energy in GaAs. As many as 16 periods were observed for magnetic field perpendicular to the GaAs layers (parallel to the current flow), while up to 30 periods were observed in magnetic fields parallel to the layers (perpendicular to the current flow).[36] The magnetic field also reduced the tunneling current, especially for the case of magnetic field perpendicular to current flow. An energy band diagram for the device studied by Hickmott et. al. is shown in figure 8. Since the barrier is very thin, and since the doping of the anode is only $1x10^{15}cm^{-3}$, most of the applied voltage drops across a depletion layer where there are no free carriers and all the donors are ionized. In order to emit a phonon, an electron must first tunnel through the barrier, then gain sufficient energy from the electric field in the depletion layer. In order to emit 16 phonons, the electron must transit the majority of the lightly doped layer, which is $1\mu m$ thick. Somehow, the emission of phonons in the lightly doped layer must affect the tunneling of electrons through the barrier.

The interpretation of Hickmott et. al. was that the periodic structure was somehow a consequence of the sequential emission of polar optical phonons by otherwise ballistic electrons in the lightly doped GaAs layer. They also suggested that the role of the magnetic field is primarily to freeze out the carriers[37] in the lightly doped region, thus eliminating impurity scattering and allowing ballistic electron transport. The carrier freeze-out was also indicated by capacitance-voltage data. This interpretation of the periodic structure leaves several problems unsolved. First, the mechanism by which the phonon emissions affect the tunneling current is unclear. Because the current density in this experiment is very small, $0.2\text{-}100x10^{-6}A/cm^2$, the space charge of carriers which only scatter by optical phonon emission is several orders of magnitude too small to account for the observed modulation of the current[38]. Also, it is not at all apparent why the structure persists at applied voltages which would correspond to 30 phonon emissions. If the sequential phonon emission hypothesis is correct, this would mean that the electron remembers its initial energy even after having emitted 30 phonons.

The puzzling results of Hickmott et. al. spurred considerable theoretical and experimental work around the world.[38-46] and focussed attention on previous experiments involving emission of phonons. Between 1958 and 1966, many workers had studied oscillatory photoconductivity in semiconductors. (For a compilation, see reference 47.) In these measurements, the intrinsic or extrinsic low-temperature photoconductivity of lightly doped materials ranging from silicon and germanium to InSb and CdS oscillated with excitation energy with period corresponding to optical phonon energies. Stocker[47] showed that the oscillations were due to a dependence of the electron distribution function on injection energy and the fact that the electron energy relaxation occurred preferentially by optical phonon emission, but the mechanism by which the distribution function affected the conductivity was a subject of debate. Stocker also showed that the oscillations disappeared in large electric fields.

In 1967, Katayama and Komatsubara[48] reported observing oscillatory tunnel conductance in InSb-oxide-metal structures. The period of the oscillations, 25mV matched the longitudinal-optical phonon energy in InSb. The oscillations were seen only at 4.2K in structures with low carrier concentrations ($n=2x10^{14}$ cm^{-3}). The only qualitative difference between the results of Hickmott et. al. and Katayama and Komatsubara is the different magnetic field dependence of the phonon structure. Hickmott et. al. see no phonon structure without magnetic field. Magnetic fields parallel or perpendicular to the current reduced both the tunnel current and the oscillations in the measurements of Katayama and Komatsubara. Katayama and Komatsubara gave two separate explanations for the oscillations.[d] One explanation is that phonons emitted after the electrons tunnel through the barrier can scatter electrons in the cathode via the long-range Coulomb interaction. A slightly different explanation is that the density of states in the anode "is modulated by the electron-phonon interaction just as in the case of polaron-induced anomalies." Essentially, this says that the possibility of multiple phonon emission allows more final states to contribute to the tunneling probability. However, this explanation is most certainly wrong. For electron densities of only $2x10^{14}$ cm^{-3} almost all the voltage applied to

[d] Katayama and Komatsubara regard the two explanations as equivalent.

the device must drop across a depletion layer, just as in the case of Hickmott's GaAs/$Al_xGa_{1-x}As$ tunnel junction. Therefore the phonon emissions must be sequential rather than multiple. Phonon emissions which occur after the electron has tunneled cannot affect the tunneling probability directly because of the great improbability of time-reversing the individual emissions.[49]

Cavenett[50] published a more detailed study of InSb tunnel junctions in 1972. He observed oscillations both in junctions made with oxide coated InSb and vacuum cleaved InSb crystals. Conduction in metal-InSb junctions occurs by tunneling at low temperatures; a Schottky barrier is formed on n-type samples. Cavenett also made junctions from crystals with different carrier concentrations and found that the magnitude of the oscillations was reduced for the higher carrier concentrations. He also found evidence in measurements using superconducting contacts that the conduction in the junctions with grown oxide occurred through pin-holes in the oxide. Conduction in junctions prepared by vacuum cleaving was probably very non-uniform as well, because the tunneling current expected through the 2000Å (as measured by capacitance) thick depletion layer is negligibly small. Cavenett proposed that the mechanism responsible for the oscillations was similar to that more or less accepted for the oscillatory photoconductivity experiments: the tunnel junction injected mono-energetic electrons into the lightly doped semiconductor, where their interaction with the optical phonons resulted in electron distributions which depended on the number of phonons emitted. The large spreading resistances associated with pinhole conduction magnified the effect of the electron distribution on the resistivity.

In light of these previous experiments, the phonon structure seen by Hickmott was not at all new. What made his results so important was that he saw the phonon effects in single crystal heterostructures grown by MBE, in contrast to the InSb junctions, whose microscopic structure was largely uncontrolled. Still, there were significant differences which made it difficult to explain Hickmott's results in terms of the InSb tunnel junction results. The most important difference was the magnetic field dependence as discussed above. Also, the current densities in the devices were dramatically different. Hickmott saw his first oscillations at a current density of about $2x10^{-7}$ A/cm^2, while one of Cavenett's junctions conducted about $0.04A/cm^2$ at its

first oscillation. These differences, and the very different structures used suggested that the phonon structure seen by Hickmott was indeed something entirely new.

Since Hickmott's work, several closely related experiments have been done. Lu, Tsui and Cox[43] at Princeton University have studied indium contacts on high purity InGaAs. These measurements are much closer in spirit to the work on InSb than to Hickmott's GaAs experiments. The current densities are large and the magnetic field dependence is similar to that reported for InSb junctions. Lu et. al. did make one surprising discovery: they saw oscillations in both current directions! To explain this, they propose that the metal semiconductor contact is made through "micro-channels" in the insulating native oxide, and that the conduction in these channels is one-dimensional. They appeal to the theoretical work of Kulik and Schekhter[51] who note that when electrons emit phonons, they slow down, causing current singularities in one-dimensional channels.[e] The oscillations are then thought to be caused by variations of the electron velocity in the micro-channels. Unfortunately, this explanation is implausible at best, because it requires ballistic transport of electrons in long channels which traverse an oxide that is at most 50Å thick. Even if such micro-channels formed, one would hardly expect them to conduct like bulk InGaAs, let alone ballistically. More likely, wide, ohmic pinhole contacts are made. The spreading resistance in these contacts is still likely to be large, but a mechanism similar to that proposed by Kulik and Schekhter may well be important, especially for the polarity where the electrons are sucked into the contact. The observation of oscillations in this polarity may also be a straightforward consequence of the comparatively huge current densities ($>1 A/cm^2$) in the InGaAs contacts. The favorable properties of ohmic contacts of In to InGaAs may have enabled the observation of oscillations in forward bias.

In more recent work, Lu, Tsui and Cox[52] studied contacts to high purity InP. These contacts were rectifying, more like the InSb contacts. In addition to the usual optical-phonon related structure, the InP contacts showed a

---

[e] It should be noted that current singularities can result directly from the velocity modulation without benefit of space charge effects as discussed below.

conductance “gap” at low temperatures. At voltages inside the gap, conductance was almost zero, while the current rose rapidly with voltage outside the gap. The gap vanished at temperatures above 10K, and widened with increased magnetic field, either parallel or perpendicular to the sample. This was attributed to the effects of carrier freeze-out. The binding energy of donors in the high mobility III-V semiconductors is of the order of 5meV in high purity material, so some electron freeze-out ought to occur at temperatures below 50K. In fact, freeze-out does occur in all of the devices I have discussed here.[f] However, even at very low temperatures, the conductivity of most material remains quite high due to impurity conduction. In very high purity material, the impurity conduction can be very small. In the InP contacts, voltages smaller than the gap voltage are insufficient to ionize any of the frozen donors, and the conductance is negligible. Higher voltages can ionize the impurities, and current increases rapidly due to impact ionization in a process similar to avalanche breakdown. (This will be discussed in more detail later.) Since oscillations are observed after the breakdown, the mechanism causing the oscillations cannot require all the donors to be frozen out. This is also indicated by the fact that Lu et. al. observed that the conductance oscillations persisted to above 77K while the conductance gap related to freeze-out vanished at 10K.

Soon after Hickmott published his work on GaAs/$Al_xGa_{1-x}As$ structures, Eaves and co-workers[53,54,41] at the University of Nottingham in England reported that they had also observed the conductance oscillations in structures similar to those used by Hickmott et. al.. In their devices, however, the oscillations were observed without magnetic field. Although their structure was almost identical to that studied by Hickmott, the Nottingham devices were in many respects more similar to the InSb, InP, and InGaAs contacts discussed above than to Hickmott's devices. As in the contact work, magnetic fields parallel to the transport had little effect other than to reduce the overall current, while perpendicular fields tended to reduce the amplitude of the oscillations. Also, the tunnel barriers in the

[f] For example, the carrier density measured by Hall effect at 4.2K in Cavenett's work is a factor of 94 less than the net impurity density measured by capacitance-voltage sweeps.

Nottingham devices were only 168Å, so their current density was several orders of magnitude higher than in the Hickmott devices. Several new phenomena were observed by the Nottingham group. They observed two types of behavior on devices made from the same wafer. The "type B" devices were similar to the "type A" devices, except for a "shoulder " on the I-V curves at low bias. Oscillations were observed both on and off the shoulder, but the shoulder oscillations were suppressed strongly by perpendicular magnetic fields. The Nottingham group also investigated the dependence of the oscillation amplitude on magnetic field in detail.[55] Using voltage modulation techniques, they observed very narrow peaks in the second derivative signal. They then swept the magnetic field while maintaining the applied voltage at the top of one of these peaks. In contrast to the monotonic increase of the peak amplitude with magnetic field seen by Hickmott, the Nottingham group finds that the peaks are resonantly enhanced at a field of about 5.1T. They cite this as evidence that impact ionization of shallow impurities is the means by which phonon emissions create space charge. This will be discussed in detail in Chapters 4 and 5.

Additional experiments have raised more questions than they have answered. Hickmott has continued his work on other phenomena in the GaAs/$Al_xGa_{1-x}As$ structures. He has reported[56] one device with oscillations of period 30mV which can be seen without magnetic field and which are suppressed in strong magnetic field. Meanwhile, the Nottingham group has found oscillations which are only seen under strong magnetic fields in a sample made in InGaAs lattice-matched to InP[57].(The InP and InGaAs play the roles of the $Al_xGa_{1-x}As$ and GaAs, respectively, in the Hickmott structure.) In this structure, the current density is similar to that in Hickmott's GaAs/$Al_xGa_{1-x}As$ structures.

Campbell et. al.[58] have very recently reported an experiment which proves beyond any doubt that ionization of shallow impurities are involved in high current density oscillations. They measured the far infrared photo-response from neutral impurities (tuned to resonance with the excitation wavelength by a magnetic field) in the un-depleted layer of a structure similar to that used by the Nottingham group. Phonon oscillations are seen without magnetic field, and the current densities are similar to those at Nottingham. They see oscillations in the photo-response with applied

voltage, indicating that the fraction of neutral donors oscillates along with the tunnel conductance.

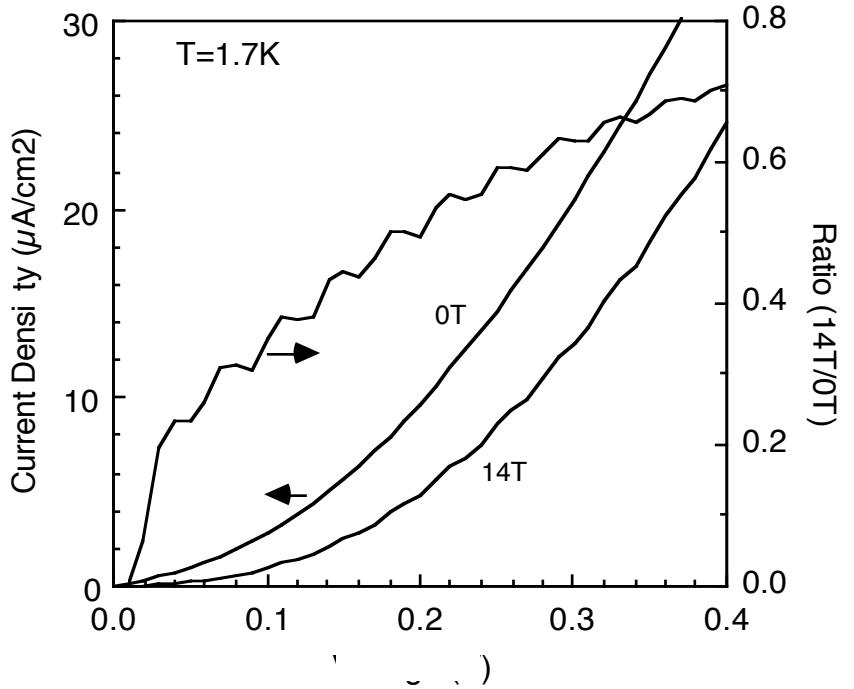

Figure 7. Current density versus voltage measured by Hickmott et. al. in tunnel barrier heterostructures, for magnetic fields of 0T and 14T applied parallel to current flow. Also shown is the ratio of the two current densities, to show the phonon structure more clearly.

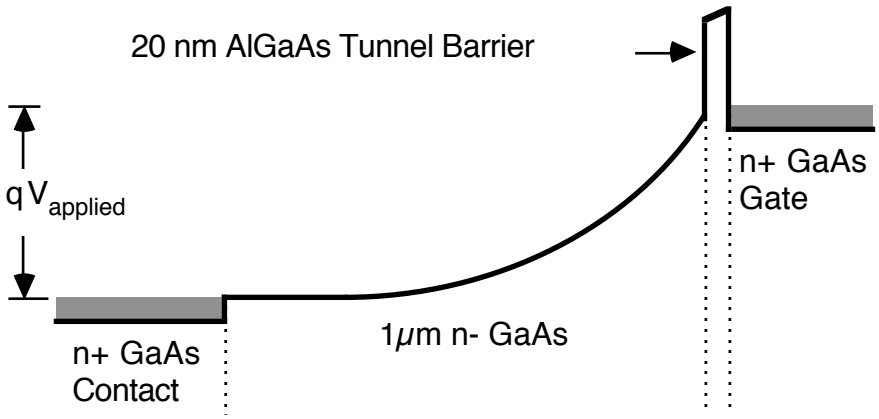

Figure 8. Schematic energy band diagram for the tunnel barrier heterostructure measured by Hickmott et. al..

3.2 Theories

Given the wealth of experiments which show the participation of optical phonons in the transport across metal-semiconductor and metal-insulator-semiconductor junctions, one might expect these systems to be well understood and uncontroversial. They are not well understood, and they have been very controversial. Since Hickmott's initial report on the oscillations, theories have become almost as numerous as theorists. The problems the theorists have worked to address are roughly as follows:

1. Are the "contact" effects the same as the tunneling effects?
2. Why are magnetic fields required to see phonon structure in some devices?
3. Why do magnetic fields suppress phonon structure in others?
4. Should the orientation of the magnetic field matter?
5. How does phonon emission affect tunneling currents?
6. Why is there still phonon structure after as many as 30 phonons have been emitted?

To answer these questions, theorists have taken a variety of approaches. As is often the case, common themes recur in several formulations. For example, some theories say that the tunneling effect and the contact effects are one and the same, while others say the two effects are unrelated. Some theories say that the magnetic field dependence of the oscillations is due to ballistic transport made possible by an absence of ionized impurity scattering when donors are magnetically frozen out. Several theories use space charge as a feedback mechanism to modulate the tunneling current. The large number of phonons observed can be explained by either electron energy coherence, in which the oscillations depend only on the electron energy, or phonon coherence, in which the number of phonons emitted determines the current modulation.

Any theory of the phonon oscillations must deal with the phenomenon of magnetic freeze-out. This effect was first studied theoretically by Yafet, Keyes and Adams[37]. In strong magnetic fields, the cyclotron radius of free electrons becomes comparable to the Bohr radius of electrons bound to shallow impurities. For GaAs, where the Bohr radius is 102Å, the Bohr radius equals the cyclotron radius at a magnetic field of 6.3T. As the field increases, the bound electron's wavefunction is squeezed so that the electron is closer to the donor, thus increasing the binding energy. At low

temperatures, the increased binding energy can cause the free carrier concentration at thermal equilibrium to decrease sharply. For uncompensated GaAs with 10^{15} cm^{-3} donors at 4.2K, the free carrier concentration without magnetic field would be $1.5x10^{12}cm^{-3}$, while according to the calculation in ref. 37, the free carrier concentration should drop to $6x10^{9}cm^{-3}$ for a magnetic field of 5T.

Hickmott suggested that magnetic freeze-out was responsible for the appearance of the phonon structure at high magnetic fields. He assumed that under conditions of magnetic freeze-out, all the free carriers in the lightly doped GaAs layer were frozen onto donors. This assumption led to the *ballistic transport* hypothesis: magnetic freeze-out leads to elimination of impurity scattering. Hickmott made capacitance-voltage measurements which seemed indicate that the donors were indeed neutralized. The capacitance measures the thickness between conducting layers. Under normal conditions, this would be the sum of the barrier thickness and the thickness of a depletion layer, in which all the donors are ionized and the carriers are swept away by the electric field. The capacitance measurements at zero magnetic field yield a depletion thickness which indicates that all the donors were ionized. This conflicts with the expectation that some of the donors should freeze-out thermally. When magnetic fields were applied, the capacitance indicates a depletion thickness equal to the entire thickness of the lightly doped layer, regardless of the applied voltage. This would imply that the donors are neutral in the magnetic fields. However, this is unlikely, because the electric fields applied to the GaAs layer during the measurements are extremely large, on the order of $10^{4}V/cm$, making it very likely that initially neutral donors are field-ionized by the measuring fields. This is confirmed by Hanna et. al.[38], who note that complete donor neutralization is inconsistent with the measured tunnel currents. The division of the undoped layer into depleted and un-depleted layers is thus simplistic. Since the carriers are likely to be frozen out throughout the lightly doped layer, this layer should be divided into a high field layer, in which the donors are ionized, and a low field layer, in which the donors are un-ionized. The measured capacitance should then depend on the conductance of the low field layer. The effect of the magnetic field may be simply to change the conductance of the low field layer. Conduction in lightly doped material takes place by hopping between impurities. This process will be very

sensitive to the magnetic field. Thus the ballistic transport hypothesis is on very shaky ground because magnetic freeze-out does not eliminate ionized impurity scattering. Even if all the carriers were frozen onto donors, real materials will always be compensated to some degree, and the compensated donors are never frozen out. (Typical material grown by MBE has an acceptor background doping of between 10^{14} and 10^{15} cm^{-3}.)

Several mechanisms have been proposed to explain how the phonon emissions can effect the tunnel current through the barrier. In brief, they are modulation of the final density of states by the electron phonon interaction, contact heating, and space charge (which comes in several flavors). The density of states modulation was proposed by Ihm in 1985[42], although a similar proposal, discussed above, had been made previously for the InSb effects by Katayama and Komatsubara.[48] Ihm treats the barrier together with the lightly doped layer as one big tunnel barrier in a scattering matrix formalism to show that the tunneling current depends on the density of final states. Because of the possibility of phonon emission, integral numbers of phonon energies could be subtracted from the initial electron energy to find the final energy. Because of a polaron interaction similar to that discussed in the Chapter 2, the density of states for a degenerate semiconductor has a sharp peak one phonon energy above the fermi level, and Ihm suggests that this peak should show up as oscillatory structure in the tunnel current. Ihm explains the magnetic field dependence by using the ballistic transport hypothesis, and indeed, he requires ballistic transport in order to be able to include the lightly doped layer in the tunnel barrier. Ihm's model is seriously flawed,[49] even without the problems associated with the ballistic transport hypothesis, for the same reason that Katayama and Komatsubara's suggestion was flawed. Because the tunneling probability is very small, inelastic events which occur after the electron has tunneled can have only a small effect on the tunneling probability; the electron must tunnel back to change the current. Furthermore, when tunneling currents are calculated, the final group velocity of the carriers must also be factored in, and this tends to cancel the density of states term.

A more reasonable hypothesis was suggested by Barker[44]. He proposes that the phonons emitted by the energetic electrons travel back to the cathode, where they heat up the sea of electrons. The heated electrons then have an increased probability for tunneling. This mechanism would give a

very neat explanation for the persistence of the structure to high biases, since the current enhancement would depend only on the number of phonons emitted (Thus *phonon coherence*). However, as pointed out by Leburton[39], the optical phonons in GaAs have an extremely short mean free path, and would almost certainly decay into pairs of acoustic phonons before getting to the cathode. Only half of these would go the right direction to get to the cathode, and once there, they would have a much lower probability of interacting with the electrons. Also, the total power was as little as 10 nW/cm^2 when Hickmott observed the oscillations. If this power were completely deposited in the cathode, the expected temperature rise should be less than $10^{-12}K$, assuming the usual lattice thermal conductivity of GaAs. For any reasonable coupling of the cathode electron temperature to the lattice, this temperature rise seems too small to cause the observed oscillations.

The recent literature expresses a growing consensus that space charge is the correct mechanism allowing the phonon emissions to influence electron tunneling through the barrier. The simplest source of space charge would be the tunneling electrons themselves. Their space charge is inversely proportional to their velocity. The high fields close to the tunnel barrier, where the donors are all ionized, should cause the electrons to travel at the saturated drift velocity, and thus the space charge close to the barrier should be negligible. Away from this region, the electric fields should be very small. In this region the velocities of the electrons are determined by their energies. Thus if an electron is injected through the barrier with 2.5 phonon energies (above the Fermi level in the collector) and emits 2 optical phonon in the ionized donor region, in the low field region it will have the velocity corresponding to 0.5 phonon energies. Since optical phonon emission is the primary energy loss mechanism for energetic electrons (until they get to the collector, where electron-electron scattering will very rapidly thermalize the electron), the energy of the electrons in the low field region of the lightly doped layer will depend almost entirely on the number of phonons emitted. In this way the space charge due to the carriers can depend periodically on the applied voltage, which determines the injected electron energy. The idea that space charge in the low field region is responsible for the oscillations is supported by the fact that the oscillations disappear at the voltage at which the entire lightly doped layer must be ionized to terminate the electric

field.[38,40] Furthermore, the bias dependence of the oscillation amplitude is modeled very well by assuming that the space charge is proportional to the thickness of this low field layer.[38]

Unfortunately the space charge due to the carriers is about six orders of magnitude too small to explain the strength of the oscillations in Hickmott's experiments. For some of the point contact experiments, however, the carrier space charge may be an entirely reasonable explanation for the observed conductance oscillations. In those experiments the currents are not only much higher, but the current flow is believed to be very inhomogeneous, leading to much higher local current densities. The recent experiments by Lu et. al. are probably similar.

Several other sources of space charge have been proposed. Leburton[39] has suggested that donors in the low field layer could be ionized by acoustic phonons created as decay products of the optical phonon emitted by the electrons. This mechanism shares the phonon explanation for coherence with Barker's contact heating hypothesis. Eaves[40] has suggested that impact ionization of the same donors by electrons is the important mechanism. Here the strong dependence of the impact ionization rate on the electron energy leads to the oscillatory dependence of the conductance on cathode voltage. The recent results of Campbell et. al. show conclusively that donor ionization from *some* mechanism is involved in the oscillations, at least in the high current density devices similar to those report by the Nottingham group. The relative importance of the two ionization mechanisms can only be determined by detailed knowledge of the resulting ionization rates. Certainly the impact ionization hypothesis is much more traditional in terms of the mechanisms which have been used to explain transport in bulk GaAs of similar purity.[59] Unfortunately, both of these explanations also require knowledge of the rates of electron capture by the donors to give a quantitative theory for the oscillations. The actual space charge will depend on a ratio of electron capture and ionization rates. Since the electron capture process is poorly understood, Leburton must assume that the capture and ionization processes are identical. This allows him to cancel out the parts which are hard to calculate, and to obtain quantitative results in good agreement with experiment.

Magnetic freeze-out fits very naturally into the donor ionization models to explain the magnetic field dependence of the phonon oscillations. Eaves

considers the low-field layer as a series resistance which depends on the energy of the incident electrons, and proposes that in Hickmott's experiment the current density is insufficient to produce a significant ohmic voltage drop across this layer. Since magnetic fields are known to increase the resistivity of lightly doped GaAs by the freeze-out mechanism, one possible explanation of the magnetic field dependence in Hickmott's data[40] is that the the currents are too small to give a significant voltage drop without the magnetic field. Although one can always describe voltage drops as ohmic, it seems rather unphysical that energetic electrons should feel the effects of freeze-out as an *increase* of the resistance, unless they are also frozen out somehow.

A major problem with Eaves' model is the mechanism of coherence of the oscillations for large numbers of phonon emissions. Wang et. al.[60] have done Monte Carlo calculations which show that because of the high electric fields near the barrier, the electrons do not all have the same energy as they enter the low field region. The phonon emission rate is not sufficient for the electrons to emit as many phonons as they might in the short time before they enter the low field layer. The spread of electron energies would thus strongly reduce any modulation of space charge dependent on electron energy. One possibility is that a polaron gap like that described in Chapter 2 causes an enhancement in the phonon emission process, thus restoring energy coherence.

One possible way to experimentally distinguish the mechanisms proposed by Leburton and by Eaves is to look for resonant processes. The phonon ionization process should be enhanced when the donor binding energy equals half of the optical phonon energy. This should occur at about 53T, or lower if electron non-parabolicity is taken into account. Impact ionization should be enhanced when the cyclotron energy equals the donor binding energy (at about 5T). The observation of this enhancement by the Nottingham group is strong evidence that impact ionization, rather than phonon ionization, is the important process generating space charge in their devices.

A closely related source of space charge was proposed by Hanna and Laughlin[61]. Instead of considering ionization of impurities, they pointed out that the capture process also depends strongly on electron energy. The capture rate should fall off very quickly with electron velocity, so that only

electrons with very small energy can be captured. This mechanism does not suffer from the energy coherence problem because although the electron energies are widely spread, the distribution functions calculated by Monte Carlo techniques have sharp peaks at multiples of the phonon energy below the initial energy.[60] When the applied voltage is such that a sharp peak occurs at zero energy, the density of electrons available for capture will rise sharply. As mentioned earlier, the capture process is poorly understood, and little progress has been made in quantifying this process.

I proposed a very different source of space charge.[46] Using the 1-dimensional polaron model described in Chapter 2, I noted that electrons with almost a phonon energy could form pinned polarons with very small velocities, especially when large magnetic fields were applied. When the pinned polarons formed, their space charge could be quite significant. The electron energy coherence is a natural result of polaron gaps in this model. Hanna, Laughlin and I used this idea to build a quantitative model for the conductance oscillations.[38] In this work, we combined the slow polaron idea with a model of inhomogeneous current flow through the tunnel barrier. We called this the "window model" because we supposed that almost all the current would flow through a thin spot in the tunnel barrier. The evidence that this is the case came from a detailed analysis of the current-voltage data taken by Hickmott. For the very small biases dropped across the tunnel barrier in these experiments, the tunneling current should theoretically be proportional to the square of the electric field at the barrier, which, using the usual depletion physics, is in turn proportional to the square root of the applied bias. Therefore, the current should be linearly proportional to the applied voltage. The actual measured current, shown in figure 7 is proportional to the square of the voltage for low biases, changing to linear for larger biases. We were able to model this behavior to very high precision using the window model. The crossover from quadratic to linear behavior should occur at a voltage which measures the size of the window (about 0.75 μm in radius). Recent data, particularly those relating the phonon oscillations to impurities, have indicated that slow polarons are probably not an important source of space charge in these experiments, however, the window model may prove to be needed to give better quantitative agreement of other theories to experiment. The factor of 10,000 increase in current density makes many of the other space charge theories more reasonable. The

observation by the Nottingham group of the type A and type B behaviors in their tunnel junctions is also very suggestive of inhomogeneous transport. The origin of the thin spots is a significant mystery remaining in the window model, however.

The role of the orientation of the magnetic field has largely been ignored by most theoretical treatments. Magnetic fields perpendicular to the current flow enhance the phonon oscillations in some experiments, while they destroy the oscillations in others. In donor ionization models, the perpendicular magnetic fields might be expected to bind the electrons more tightly against the electric fields, thus enhancing the oscillations. The same would be true for free-carrier and slow polaron space charge models. Perpendicular magnetic fields might be expected to damp the oscillations either by reducing the current density or by inducing Hall fields which destroy the energy coherence in samples with point-contacts or inhomogeneous tunneling. To account for both types of behavior will require different models for different experiments.

We must regard the theoretical understanding of the phonon structure in the tunneling experiments as limited at best. There is some agreement that space charge in a low field layer is responsible for the structure. Although impact ionization of neutral donors appears to be involved in some of the devices, the origin of the space charge in Hickmott's devices has not been determined. There is agreement that the deepening of the donor energy by the magnetic field has something to do with the magnetic field dependence of the effect, but that complete donor neutralization does not occur. And finally, it seem clear that inhomogeneous transport occurs in at least some of the experiments. Whether one physical origin can explain the entire range of experiments remains to be determined. Since the interesting physics appears to occur in the lightly doped GaAs layer rather than in the tunnel barrier, a closer examination of the transport processes in this material is warranted, especially in the case of longitudinal magnetic fields. The next chapter will describe experimental work on transport in lightly doped GaAs in large magnetic fields.

4. Hot Electron Transport in Parallel Magnetic Fields

4.1 Motivation

In Chapter 2, I discussed the possibility that strong magnetic fields could give rise to new, 1-dimensional transport phenomena by changing the way that electrons interact with and emit phonons. In Chapter 3, I discussed experiments in which new phenomena related to phonon emission were observed when magnetic fields were applied. I described an attempt to link the theory with the experiments, but the supporting evidence is less than overwhelming. While arguments can be made that energy coherence in the tunneling experiments requires some sort of polaron effect, it would be more satisfying if the one dimensional effects of Chapter 2 could be found in a new experiment. In addition, the heterojunction experiments point to interesting things happening in the high purity GaAs layer found in these devices.

To investigate these possibilities, I decided to study electrical transport in bulk layers of high purity GaAs. By applying relatively large electric fields, I could study transport of energetic electrons, which is dominated by phonon emission. Magnetic fields could then be applied to look for 1-dimensional effects. The rest of this chapter describes these experiments in detail.

4.2 High Purity GaAs

High purity material was necessary for these experiments for several reasons. In order to see the 1-dimensional effects, broadening due to impurity scattering must be small compared to the relevant energies for the 1-dimensional effects. These would include both the cyclotron energy and the polaron gap energies. The phonon effects for the heterojunction experiments also were most pronounced for materials with higher purity. The impurity freeze-out effects are known to be observable only for material with low impurity concentration, because of the possibility of inter-impurity conduction.

Although molecular beam epitaxy has been used to grow epitaxial layers of relatively high purity GaAs, the background impurity concen-

trations in these layers have usually ranged between 10^{14} and 10^{15} cm^{-3}. Thus, the lightly doped layer used in the structures of Hickmott and of the Nottingham Group is roughly the lowest doping which can routinely be grown by MBE. At this doping level, the compensation by background impurities is expected to vary significantly from MBE machine to MBE machine and even from run to run in a single machine.

The MBE group at Stanford has made a considerable effort to stretch the limits on purity imposed by MBE.[62] The predominant background impurity species for clean GaAs MBE systems is carbon, which incorporates as an acceptor under the usual growth conditions. Carbon persists in an ultra-high vacuum environment in the form of hydrocarbons and carbon monoxide which are particularly common and difficult to remove from the vacuum chamber. To reduce the carbon background in our MBE system, standard bake-out techniques were pushed to their limits. For example, the furnaces were fired at 1600°C for several hours. The opening time for the chamber was kept to a minimum. The uncooled source area was heated overnight by firing furnaces to 748°C. The bake-out of the vacuum chamber itself was extended to more than a week, and careful insulation of the bake-out shrouds allowed us to push the temperature of this bake to 211°C, as measured at the substrate heater thermocouple. The outer surface of the vacuum chamber was discolored slightly by the bake. After the bake-out process, the principle residual gases were not carbon and oxygen, as is usual, but rather chlorine, which was introduced by the procedure we used to clean our gallium source material.

Apart from system cleanliness, the principle limitation to the purity of MBE GaAs has been the purity of the source materials. We used a 8Nm grade frozen gallium ingot obtained from Allusuisse, and a solid slug of 6N+m grade pure arsenic manufactured by Furukawa. Despite the fact that this source material was the best available, we found that after reducing the residual carbon in our chamber, we were limited by impurities in the arsenic. These were identified as sulfur, which is a shallow donor in GaAs.[63] Temperature dependent Hall mobility measurements indicated that our best nominally undoped material was n-type with a donor concentration of about $1.5 \times 10^{14} cm^{-3}$, and a background acceptor concentration of only $2.5 \times 10^{13} cm^{-3}$. The peak mobility measured in this material was 216,000 cm^2/Vs at 46°C, which is the highest mobility ever reported for GaAs grown

by MBE. To obtain the low donor concentration, this layer was grown with an arsenic flux which was the minimum required to obtain arsenic stabilized growth. Detailed information about the growth procedure is given in reference 62.

Other factors probably played a very important role in the achievement of this high mobility GaAs. The Stanford MBE system was one of the first to be equipped with a substrate holder compatible with 3 inch substrates and direct radiative substrate heating.[64] The new method of mounting and heating substrates is much cleaner than the older method of soldering substrates with indium and heating them conductively. Contaminants dissolved in the liquid indium during the soldering procedure can reduce the purity of epitaxial material. Even with the indium free holders, significant amounts of contamination are carried into the growth chamber on substrate holders. After they are loaded into the MBE system load lock, substrates are heated under vacuum to desorb water, oxygen and other surface contaminants. We found that increased pre-heat temperatures and times resulted in significantly improved epitaxial layers. In one experiment, modulation-doped layers were grown on substrates which had been baked out at 400°C for 1 hour. The two wafers were then baked at 695°C and at 400°C, respectively, for an hour under arsenic flux in another chamber. The resulting mobility was 138,000cm^2/Vs at 77K for the wafer which had had the extra 695°C pre-bake, compared to 99,000cm^2/Vs for the wafer with 400°C bake. Substrate handling procedures and hardware which prevented substrate holders from touching anything other than cleaned metal surfaces also substantially improved the general material quality produced by the MBE system.

For the transport experiments, I grew a 3.0μm thick layer of GaAs with nominally $1x10^{15}cm^{-3}$ of silicon doping. This doping was chosen to be the same as that used in the lightly doped layer of the heterojunction experiments, and because lighter doping would have required the growth of a much thicker layer, which would have complicated the subsequent processing. This substrate was outgassed at 467°C for 30 minutes and then at 695°C for 5 minutes in the load chamber. The surface after this treatment was slightly cloudy, probably due to preferential arsenic loss. After the substrate was transferred to the growth chamber, its temperature was measured as a function of heater power using infra-red transmission

spectroscopy.[65] During this process, the substrate was exposed to a flux of arsenic, and the surface became shiny again. A streaky RHEED pattern showing a reconstructed surface indicative of a smooth, clean surface was observed before any GaAs was grown. The substrate temperature during growth was 645°C, the As/Ga flux ratio was 13 (gauge pressure) and the growth rate was 1μm/hr.

The actual thickness of the layer was determined by the angle-lap and stain technique to be about 3.04μm. Hall measurements using a sample of the van der Pauw geometry indicated a sheet carrier density of $3.4\text{x}10^{11}\text{cm}^{-2}$ at room temperature and $4.2\text{x}10^{11}\text{cm}^{-2}$ at liquid nitrogen temperature. The higher carrier density at 77K may be due to ionization of deep traps in the substrate or at the growth interface. Adjusting for the surface and substrate depletion,[66] the carrier concentration is determined to be $2.43\text{x}10^{15}\text{cm}^{-3}$ at 77K. The mobility was $7780\text{cm}^2/\text{Vs}$ at room temperature and 56,700 cm^2/Vs at 77K. Using the calculation of Wolfe et. al. .[67] this mobility would indicate a compensation ratio of 1.3 and a background acceptor concentration of $4\text{x}10^{14}\text{cm}^{-3}$.

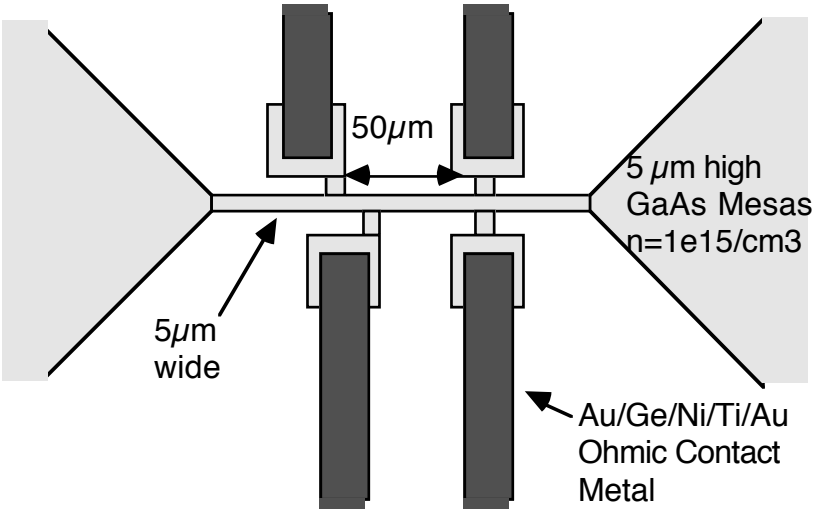

Figure 9. Layout of the GaAs resistors used in this study. Current is forced through the tapered end contacts, while electric fields are measured with the side contacts. The structure is isolated by the semi-insulating substrate. The lines of ohmic contact metal go to bonding pads at the edge of the chip.

4.3 The Experiment

In order to apply high electric fields to the GaAs layers while minimizing power dissipation and applied voltages, the epitaxial layers were

patterned into small resistors with tapered current contacts at the ends and small arms along the side for parallel and transverse field contacts. The layout for the resistor is shown in figure 9. Photoresist was patterned into the hourglass resistor shapes with necks 10μm (mask) wide and 200 μm long. The spacing between the field contacts was 30 and 50 μm on either side. The photoresist was used as an etch mask for a 3:1:50 $H_3PO_4/H_2O_2/H_2O$ mesa etch. The final width of the resistor was 3.8μm on the top and 6.2 μm at the base, as measured by SEM. AuGeNi/Ti/Au metallization was deposited and patterned by lift-off using a plasma hardened two layer resist. This metal layer was used both to make ohmic contacts to the doped GaAs mesas, and to form wire bonding pads. After an anneal of the ohmic contacts in H_2 at 450°C for 5 minutes, the wafer was diced. Dice with well formed resistors and no growth defects close to the resistors were selected for electrical test. These dice were then mounted in non-magnetic ceramic packages, and the appropriate pads wire bonded. The experiments described below used six of these resistors, all from the same wafer. These resistors were identical except for small variations in width.

Electrical measurements were done at liquid helium and at liquid nitrogen temperatures. Packaged samples were mounted with thermal grease in parallel and perpendicular field positions on a copper cold finger which was placed in the bore of a superconducting magnet. Temperatures near liquid helium were measured by carbon glass resistors mounted close to the samples. A calibrated GaAs resistor was used near liquid nitrogen temperatures. Currents were forced through the large contacts at the ends of the resistor, and voltages were measured at the side contacts using an electrometer with input impedance greater than 100 GΩ or using a multimeter with input impedance of 10 MΩ. For the perpendicular field configuration, the Hall (transverse) voltage was also measured. Current-voltage data were collected automatically by an IBM PC-AT running ASYST data acquisition software, and then transferred to a Macintosh for data analysis and graph generation.

Instabilities due to substrate effects made it impossible to reproduce the resistivity measurements precisely. At room temperature, the voltages were unstable above a critical applied voltage, typically about 40V. Measurement of significant zero-magnetic-field transverse voltages showed that this was

due to the injection of current into the substrate.[g] Deep traps (named EL2) in the substrate are responsible for its semi-insulating character, but can also give rise to effects such as back-gating in MESFET's.[68] Thus, when electrons are injected into the substrate, many of then can be trapped there, and thus change the amount of substrate depletion in an epitaxial layer. At room temperature, the instabilities due to the substrate injection have time constants ranging from a few milliseconds to a few seconds. At lower temperatures, the time constants are much longer, so that measurements are repeatable as long as no current is injected into the substrate. For this reason, the compliance voltage of the current source was monitored to avoid substrate injection at the contacts, and the measurement software was written so that the the resistor spent a minimum time under bias. However, substrate injection could not always be avoided, as it was desired to measure electric fields as high as possible. A backside bias to suppress the substrate injection was applied on some samples with intermittent success. Another technique was to use a light emitting diode to depopulate the traps in the substrate at low temperatures.

At helium temperature, the substrate injection problems were even worse because of carrier freeze-out. This caused the substrate to have a resistivity similar to that of the epitaxial layer. Once a few of the impurities in the doped layer were ionized, however, the measurements proceeded easily.

Contact freeze-out was another nagging problem for the measurements. Even at liquid nitrogen temperature, where the resistivity of the GaAs was relatively low, the ohmic contacts, when left alone for a while, would become very resistive. Usually this problem went away when currents flowed through the contacts. This problem became more serious at helium temperature, but light from the diodes usually allowed the measurements to proceed.

---

[g] Since the resistor itself is symmetric, the transverse voltage should be zero in the absence of a magnetic field. However, the metal lines from the field contacts wrap around the resistor in an asymmetric way, so that substrate current induces apparent transverse voltages.

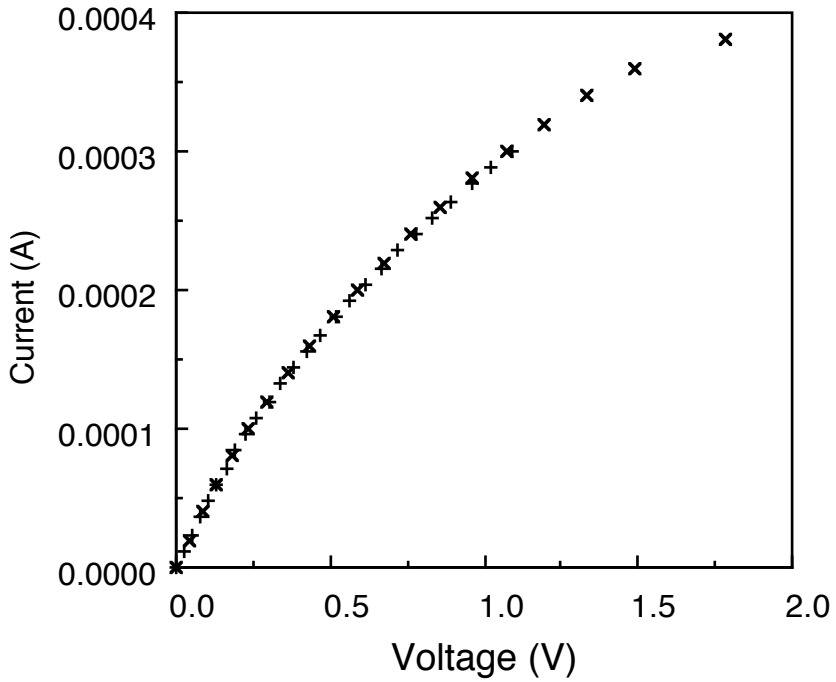

Figure 10. Four-point current-voltage characteristic for a typical resistor, measured at 93K without magnetic field. Data from two consecutive measurements (+ and x) show excellent repeatability.

4.4 Results

4.4.1 Current-Field Measurements

A typical current-field characteristic at 93K with no magnetic field is shown in figure 10. At low electric fields, the curve is linear, while for fields above 100V/cm, the differential resistivity increases. The two sets of data shown in figure 10 where taken consecutively on the same sample, and show excellent reproducibility. Other measurements made under the same conditions, but at different times were not so reproducible, because of the instabilities mentioned above. The low field resistance showed long term drifts of more than 50%. As an example, figure 11 shows a series of measurements under similar conditions for a single resistor. There is no systematic dependence of the resistance with temperature or any other measurement parameter. In order to interpret the current-field data without having to take into account the random variations in resistivity, I plot the logarithmic derivative of the current, $\partial \ln(I)/\partial \ln(E)$, rather than the current itself. Figure 12 shows the same data as in figure 11 transformed in this way.

A logarithmic derivative of one corresponds to linear behavior, while smaller values indicate sublinear behavior. Thus, the logarithmic derivative of the current vs. field curve can be termed the conductivity exponent. Figure 12 thus gives a much better picture of the relative shapes of the current-field curves without regard to the absolute magnitude of the resistivity. The conductivity exponent plots, unlike the current-field plots, are reproducible for a given sample. Note that the logarithmic derivative, or conductivity exponent, drops sharply at a relatively low field, and then has a shoulder between 100 and 500 V/cm. Figure 13 shows a similar plot for a second sample which was measured up to higher electric fields. In addition to the initial drop of the conductivity exponent and the intermediate field shoulder, a second fall-off is seen in the conductivity exponent above 500V/cm.

Figure 14 shows two non-consecutive conductivity exponent plots for a single sample at 80K with a parallel magnetic field of 7T. Although the shape of the curves are similar to those observed without magnetic field, there are significant differences. The current field curves are slightly superlinear at fields below about 100V/cm. Figure 15 shows data measured on one sample at magnetic fields of 0T, 4.5T and 7T all on one plot. In this graph it can be seen that the second fall-off of the conductivity exponent in the high field region is only observed for zero magnetic field. Although it isn't indicated in the logarithmic derivative plot, the low field resistivity increases by about a factor of two from zero magnetic field to 7T. Since the electron mobility is not expected to change due to parallel magnetic fields, this is a clear indication that magnetic freeze-out is occurring, even at 80K.

The effect of perpendicular magnetic fields at liquid nitrogen temperature is best shown by calculating the mobility and sheet carrier density in the usual way. Figure 16 shows both the apparent Hall mobility and the sheet carrier density versus electric field for a magnetic field of 7T. A width of 5μm is assumed for the resistor, although the effective width is probably smaller. Since the Hall fields are at least ten times larger than the longitudinal fields for this high magnetic field, it is not clear that a standard Hall analysis applies. Both the mobility and carrier density are considerably smaller than measured at small magnetic fields. The current field characteristics are very non-linear at low fields. This behavior is shown in the logarithmic derivative plot in figure 17. Note again that no fall-off of the

conductivity exponent is seen at high fields.

Current-field characteristics at liquid helium temperature were more difficult to measure reproducibly. Figure 18 shows a series of current-field curves measured consecutively without magnetic field, but with different current ranges and measurement intervals. The turn-on behavior appears to depend on the measurement interval, indicating a time dependence of the turn-on. Note that above the turn-on field, the curves are roughly resistive. This can be seen in the plot of the conductivity exponent in figure 19. The expanded plot in figure 20 shows the very large exponent measured at a critical field of about 4V/cm.

When parallel magnetic fields were applied at liquid helium temperature, the field required to turn on the conductance increased dramatically, as seen by comparing figure 21 to figure 18. The turn-on voltages were very asymmetric for positive and negative currents. This indicates that significant voltage was dropped across the voltage contacts. (The current field curves had to be measured using the multimeter with 10MΩ input impedance because the electrometer was too slow.)

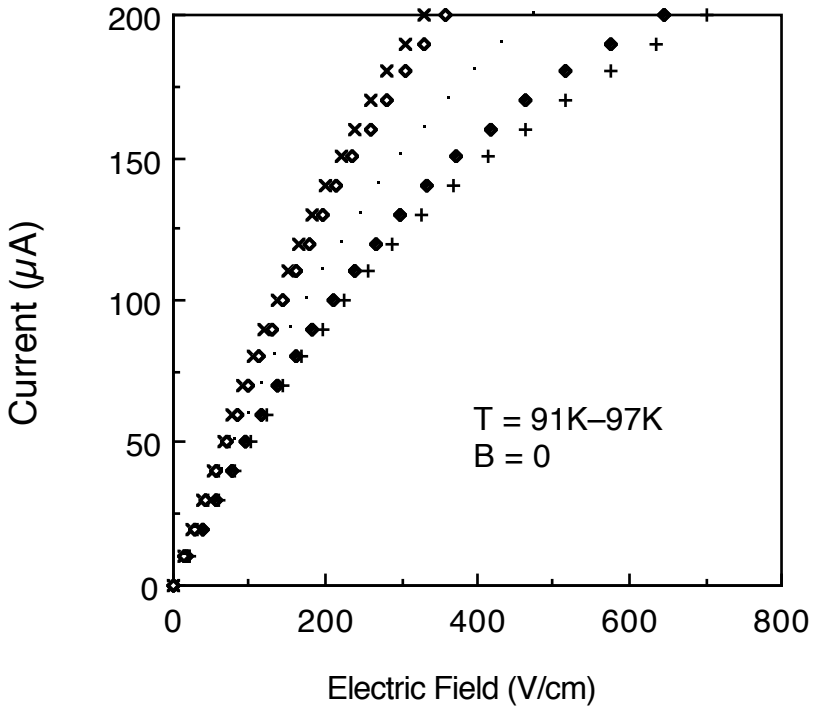

Figure 11. Current versus electric field for a single GaAs resistor measured at several times. The low field resistance varies widely, even after accounting for the small temperature variations.

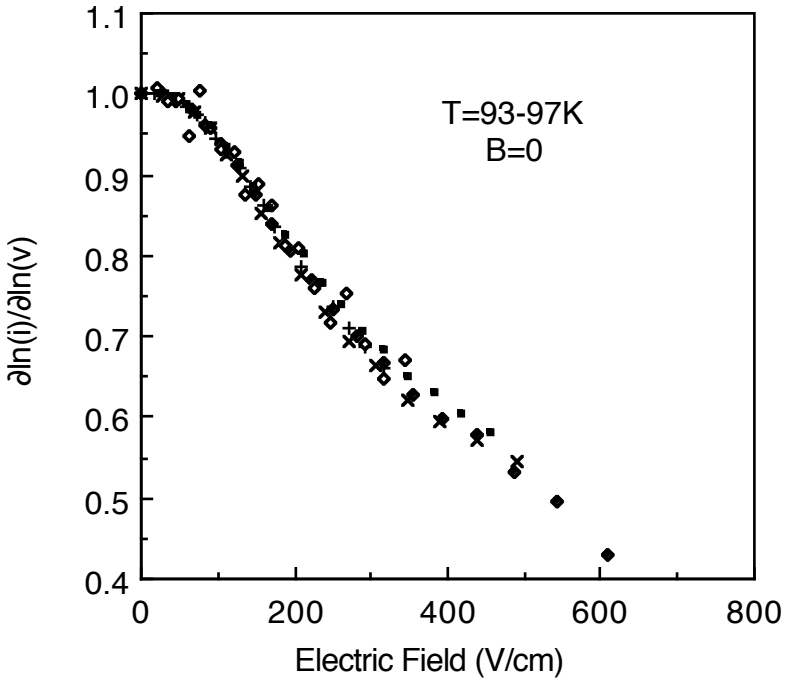

Figure 12. Conductivity exponent versus electric field for the data of figure 11. Despite the variation in the current field curves, all the data maps onto one curve.

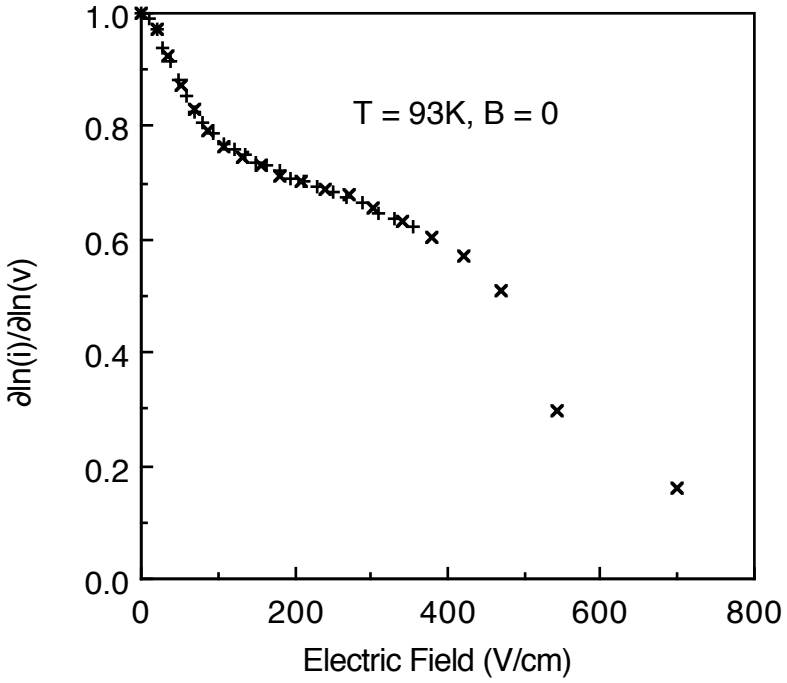

Figure 13. Conductivity exponent versus electric field for a resistor which was successfully measured up to 1kV/cm. Note the second drop-off above 600 V/cm.

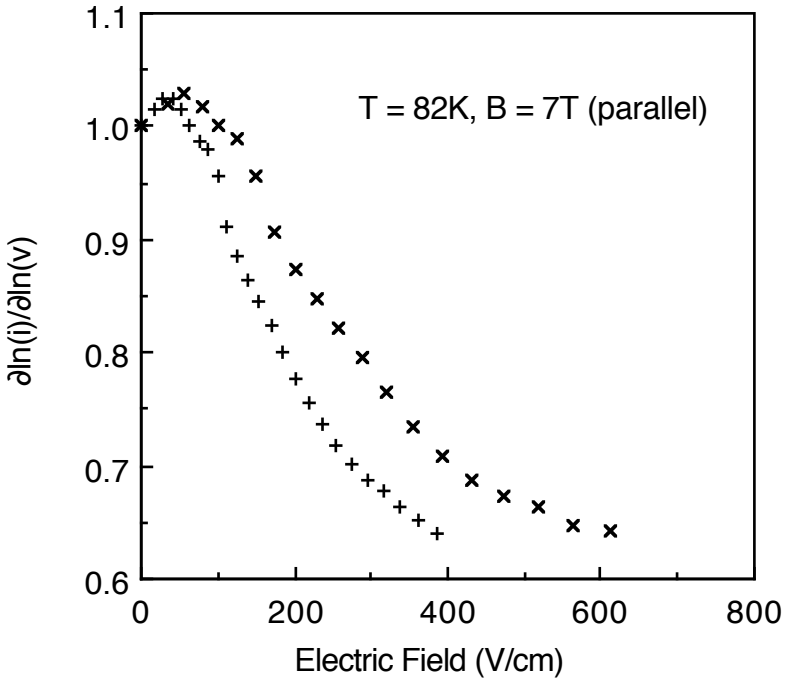

Figure 14. Conductivity exponent versus electric field for conduction parallel to a 7T magnetic field. Note the superlinear behavior (exponent >1) for fields less than 100V/cm. The two curves are non-consecutive measurements of a single sample under identical conditions.

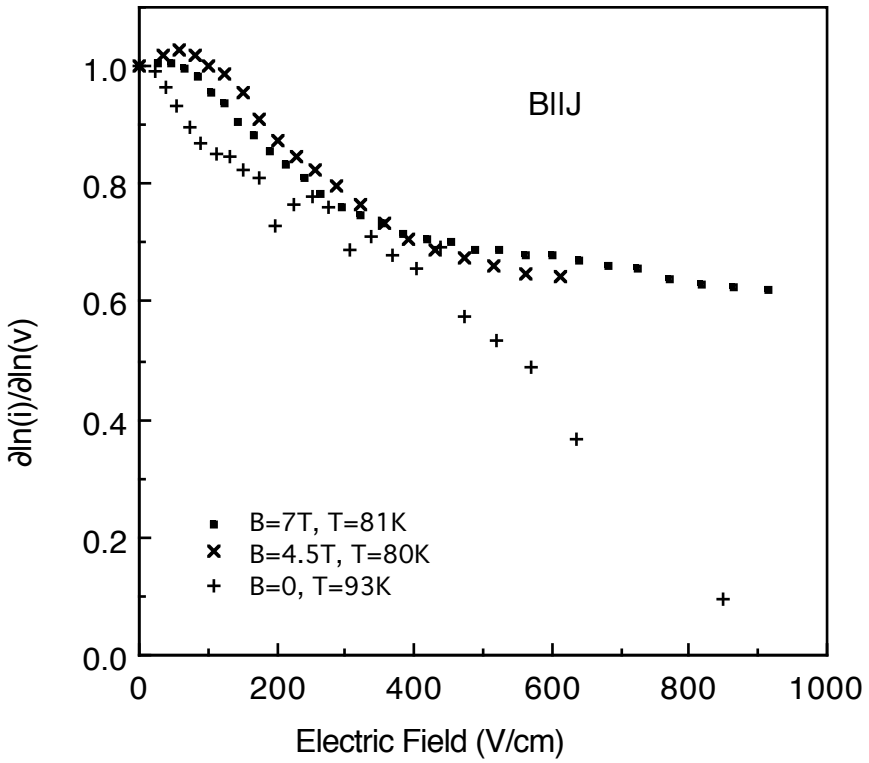

Figure 15. Conductivity exponent versus electric field for measurements of a single sample made in parallel magnetic fields of 0T, 4.5T and 7T. Note that the exponent falls below 0.6 for fields greater than 600 V/cm only for the measurements made without magnetic field.

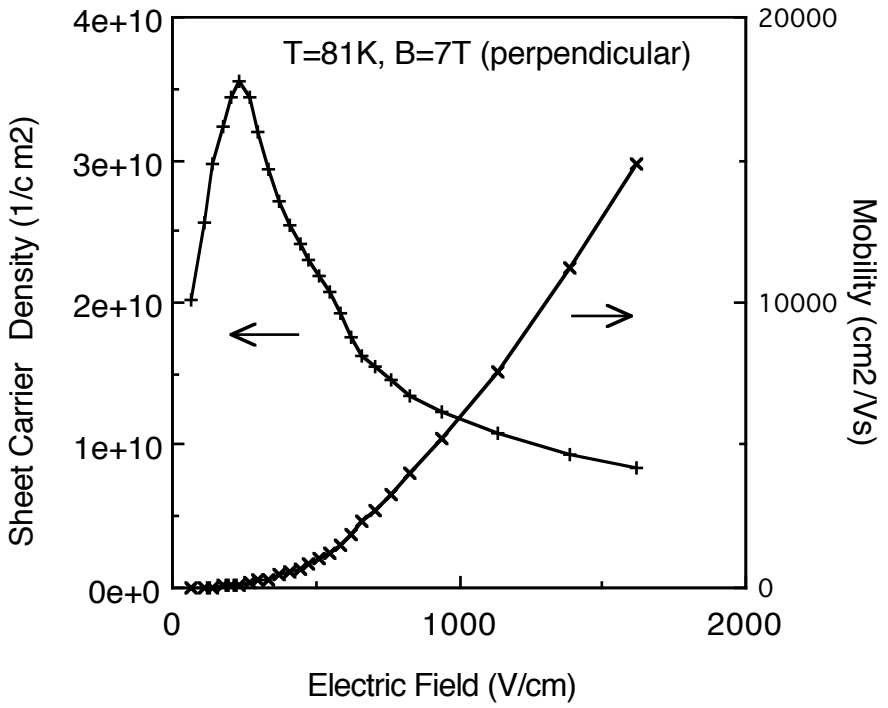

Figure 16. Apparent Hall mobility and sheet carrier density as a function of electric field derived from the current field measurements in perpendicular magnetic field. A width of 5μm is assumed for the resistor, although the effective width is smaller.

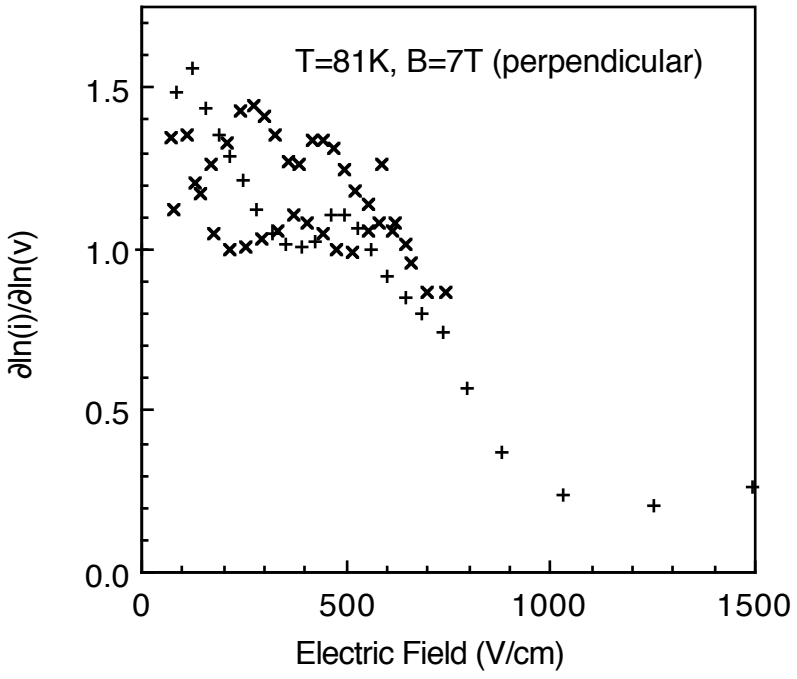

Figure 17. Conductivity exponent versus electric field measured on a single sample with a 7T magnetic field perpendicular to the current. Note the wide variation in the superlinear behavior, which extends up to 600V/cm.

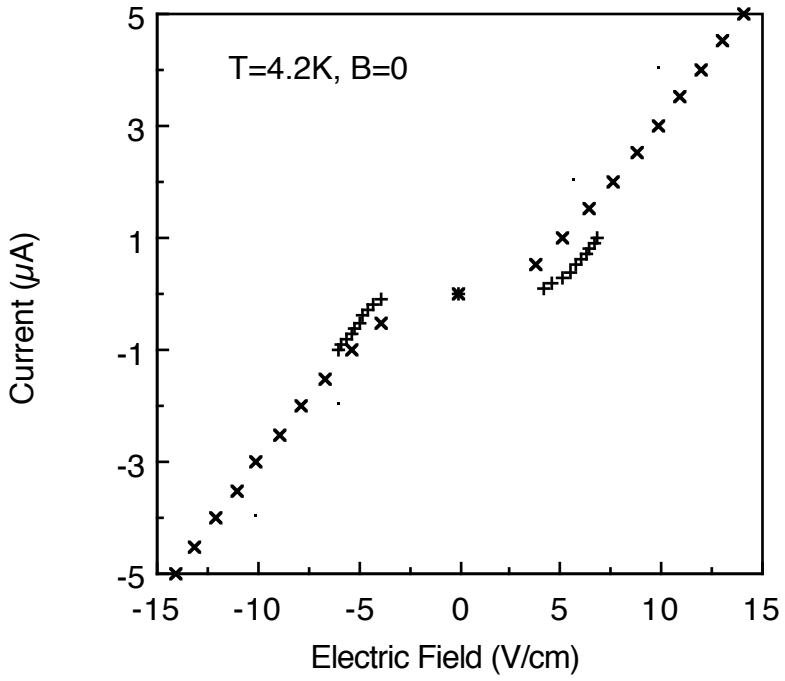

Figure 18. Current versus electric field at liquid helium temperature. The different measurements were identical except for the current step. Current flows above a critical field of about 4V/cm.

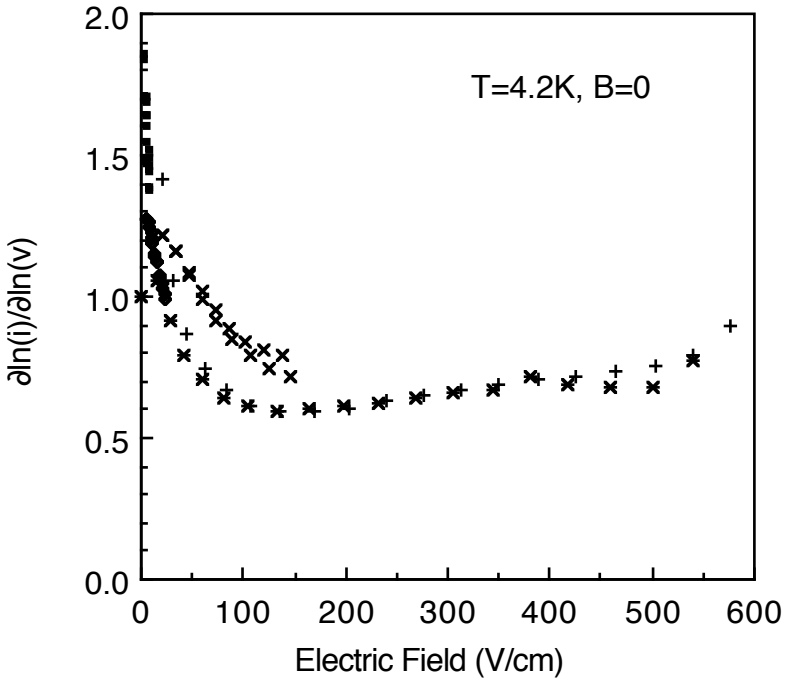

Figure 19. Conductivity exponent versus electric field at 4.2K. Weak superlinear behavior continues up to 100 V/cm.

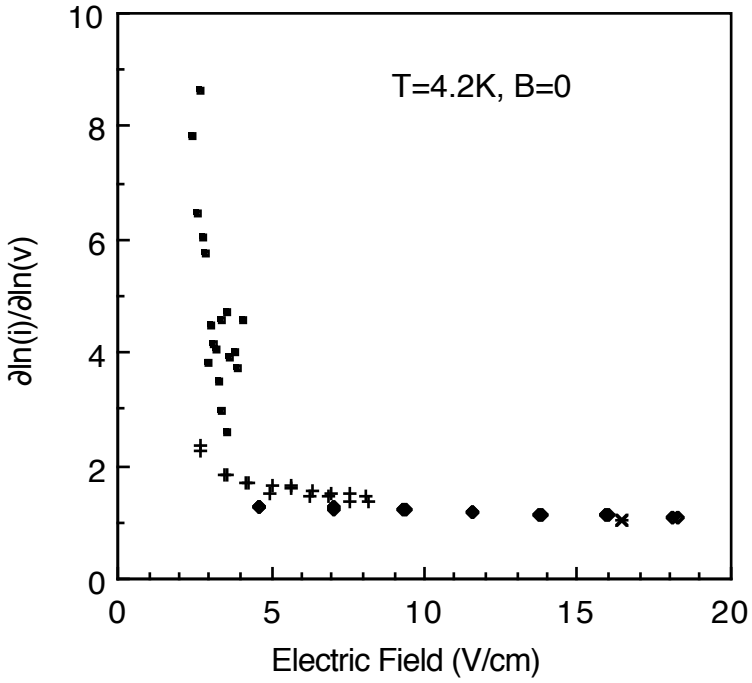

Figure 20. Behavior of 4.2K conductivity exponent at low fields. The 4V/cm critical field is seen clearly as a sharp break-point in the curve.

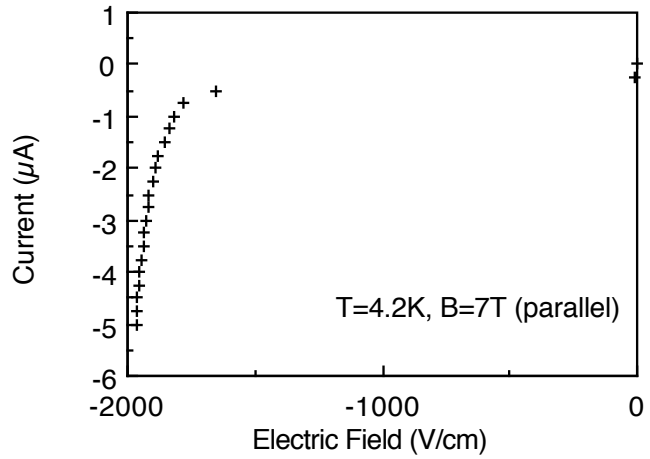

Figure 21. Current versus electric field with 7T parallel to the current. The asymmetry of the curve may be due to voltage drops in the contacts.

4.4.2 Magnetic Field Sweeps

Sweeps of the magnetic field from 0 to 8.5T were made to get a better picture of the magnetic field dependence of the conduction at liquid helium temperature. By fixing the current and measuring sufficiently slowly, it was

possible to use the very high input impedance electrometer to do the field measurements, thus reducing voltage drops at the contacts. These sweeps reveal a remarkable oscillatory longitudinal magneto-resistance. Figures 22 and 23 show the measured resistance as a function of parallel magnetic field for two different samples at a variety of applied currents. In figure 22, a minimum is observed near 5T, while maxima are observed at 2.7T and at 7.5T. There appears to be some hysteresis in the curves; this may indicate that the sweep rate, ~.5T/min, was too fast for the system to reach steady state. Similar structure is observed for a second sample measured in identical conditions, shown in figure 23. The .5μA curve in figure 23 resembles the 5μA curve in figure 22, both in the shape and the magnitude of the resistance. A minimum between 4 and 5T is observed in the 2μA curve. In both samples, larger currents reduce the resistance and the amplitude of the magnetoresistance variation. A significant increase of noise in the voltage measurement was observed for magnetic fields above about 5T.

Oscillatory magneto-resistance was only observed for parallel field geometries when the sample had a roughly resistive behavior above a critical field, and small zero-field transverse voltage. When the on resistance was very low, no reproducible structure was observed. Samples mounted in perpendicular field all showed significant zero field transverse voltages, indicating either substrate conduction or voltage drops in the contacts. The magnetoresistance (ρ_{xx}) for 2 measurements, sweeping magnetic field down and up, on one sample is plotted as a function of magnetic field in figure 24. Minima in the magneto-resistance similar to that seen for parallel field are observed between 4 and 4.5T, while a second minimum, occurs at about 7T. These curves can also be interpreted as having maxima at 3.3T, 5.2T and 8.5T. Less pronounced structure is seen in the Hall voltage at the same fields. Figure 25 shows similar measurements on the same sample, but with a smaller current. A prominent minimum in both ρ_{xx} and ρ_{xy} occurs at 2.5T, while structures corresponding to those seen in figure 24 are very weak or absent. The apparent absence of the usual magnetic field dependent Hall Voltage is somewhat surprising as well. It may be a sign that conduction in open orbits along the sidewalls of the Hall bar may dominate the perpendicular field conduction when the bar is narrow.

No magnetoresistance structure was observable in the same devices at liquid nitrogen temperature, or during measurements of much larger Hall

bars fabricated from the same wafer as the devices described above. The latter measurements appeared to be hampered by very large resistances in the voltage contacts.

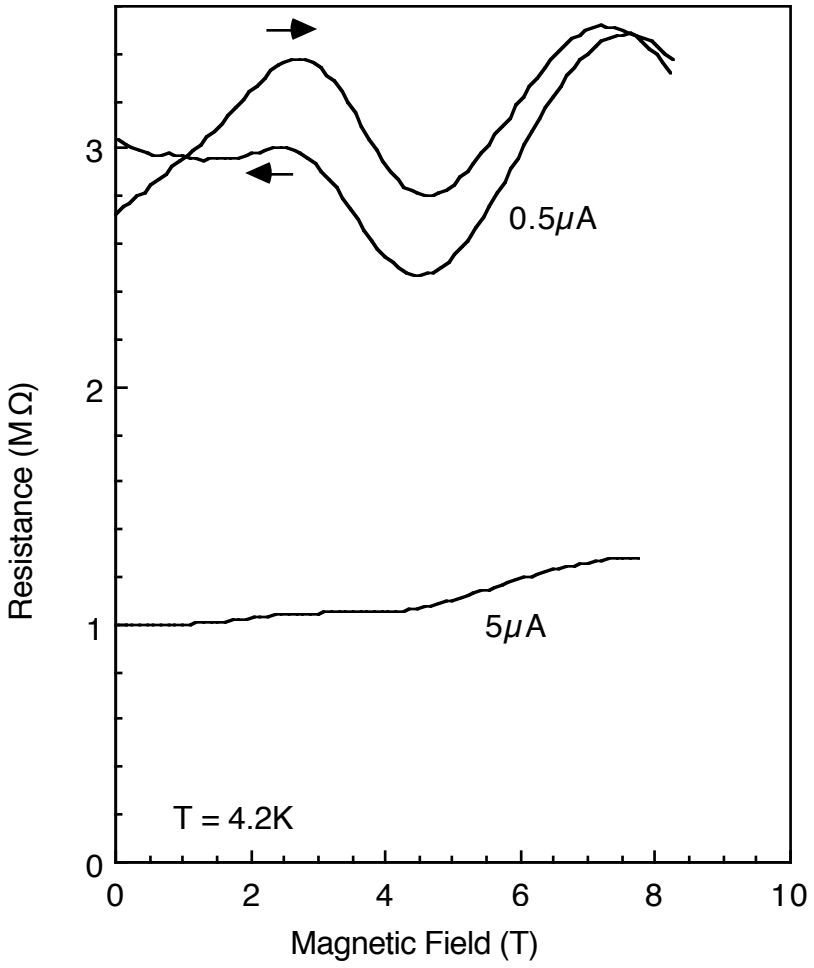

Figure 22. Longitudinal magnetoresistance as a function of the magnetic field, for two applied currents. The two traces at the top are for magnetic fields sweeping up and down.

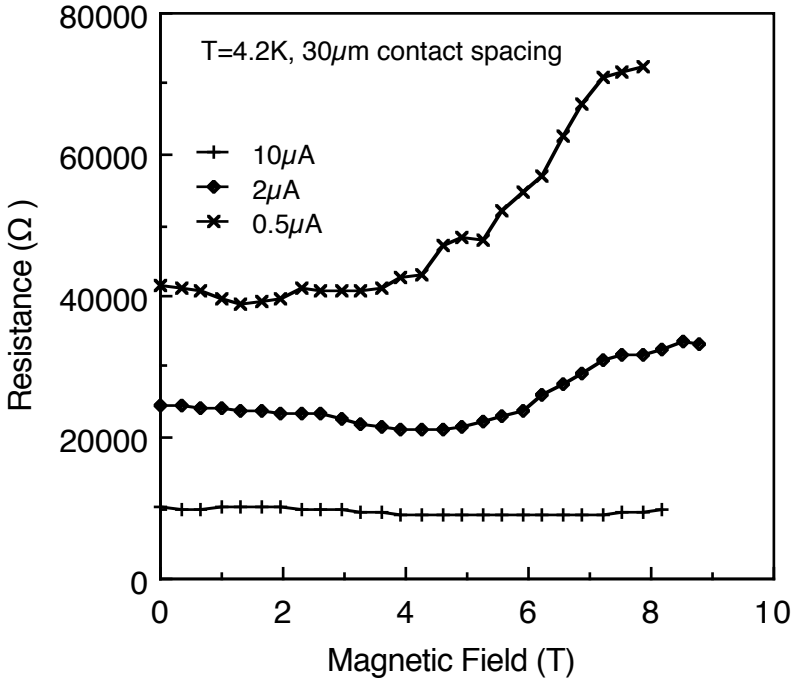

Figure 23. Longitudinal magnetoresistance as a function of magnetic field, for three currents, in a second sample. Note that the resistances are considerably lower in this second sample.

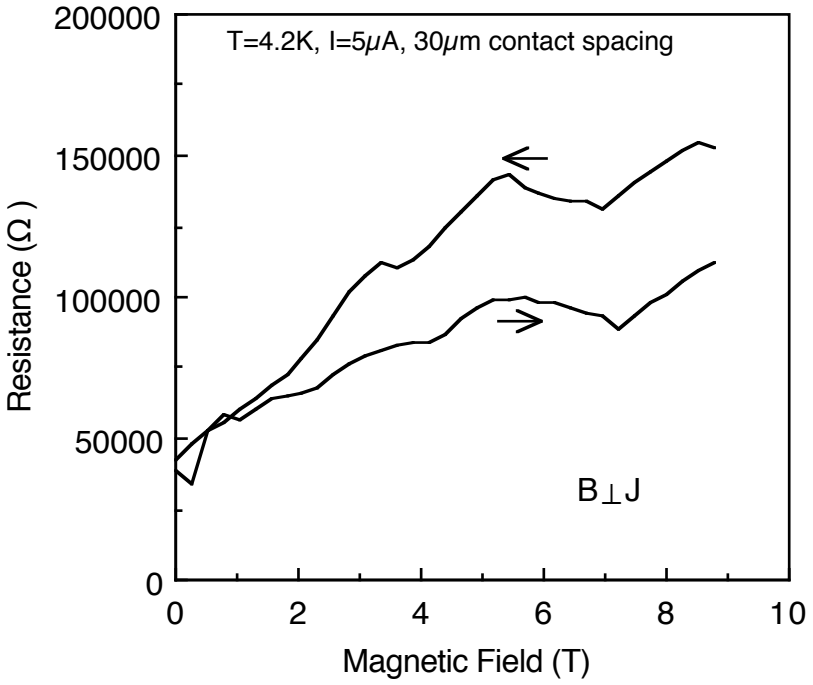

Figure 24. Transverse magnetoresistance, ρ_{xx} versus magnetic field for a current of 5μA, magnetic field sweeping down and up.

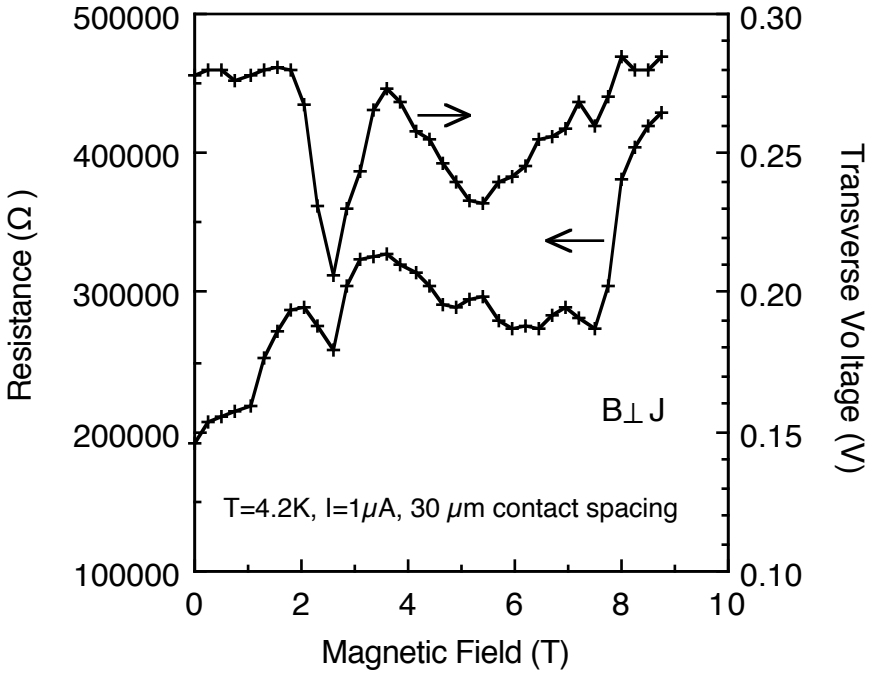

Figure 25. Transverse magnetoresistance, ρ_{xx} , and transverse (Hall) voltage versus magnetic field for a current of 1μA.

4.5 Analysis

4.5.1 Electron Heating

The principal feature of the current-field characteristics measured above liquid nitrogen temperature in the absence of magnetic field is the increase of the resistivity with increasing electric fields. This behavior is well known[69] and is due to the heating of electrons by the electric field. High field electron transport in GaAs has been of wide theoretical and experimental interest since the discovery of the Gunn effect at even higher fields. More recent work has concentrated on the possibility of transient velocity overshoot in moderate electric fields (3-10 kV/cm) which are quickly modulated either in time (<10ps) or in space (<500Å). The range of fields studied in the present work is properly referred to as the "warm" electron range, because the electrons are not hot enough to undergo the inter-valley transfer processes which give rise to the Gunn effect. The lattice temperature range is "cold" because impurity scattering dominates in small electric fields. Surprisingly, the warm electron-cold lattice regime of electron transport has not been a subject of careful measurements or theoretical modelling. It lies in a combination of lattice and carrier

temperature ranges in which neither low-temperature nor high-temperature approximations apply. In contrast, the warm electron, warm lattice range has been studied extensively,[69] but calculations are much simpler because both low and high field transport are dominated by lattice scattering. The usual low-field approximation used for the warm electron regime is a Taylor expansion of the mobility around its zero field value:

$$\mu = \mu_0 (1 + \beta E^2) \qquad (16)$$

where β is called the warm electron coefficient. Figure 26 shows a logarithmic derivative plot of the data from figure 10 along with a fit of equation (16) to the current-field data. The logarithmic derivative plot shows that the fit is poor for this range of electric fields. Monte Carlo calculations by Ruch and Fawcett[70] which extend down into the warm electron regime are the only published quantitative calculations which apply.[h] Since the published Monte Carlo calculation applies only for a specific set of sample parameters, we are without an established model with which to interpret the experimental data of Chapter 3. Instead, I will consider the behaviors of a few simple models for the effects of electron heating on the resistivity, and use them to sketch a qualitative picture of the transport mechanisms from the experimental data.

Wolfe and Stillman[71] have calculated the relative importance of various scattering mechanisms for the low-field electron mobility in high purity GaAs. The two most important mechanisms are ionized impurity scattering and polar-optical phonon scattering. At temperatures above about 100K, the phonon scattering dominates the mobility, while at temperatures below about 50K, the ionized impurity scattering dominates. The phonon scattering dominates at high temperatures because of the increased population of thermal phonons and because impurity scattering becomes less effective with increasing electron temperature. Energetic electrons, whether produced by large electric fields or by higher lattice temperatures are scattered less effectively by ionized impurities. However, they suffer additional scattering by processes which are not possible for less energetic electrons. The most

[h] The calculations of Ruch and Fawcett do not work well for warm electrons because the electrons transit the finite volume used for the calculation too quickly.

important of these processes is polar-optical phonon emission. Electrons with energy greater than 36 meV emit phonons at a rate of about 2×10^{13}/s (see fig. 3). A model for warm electron transport must take this process into account.

How can the phonon emission process be incorporated into a model for the warm electron mobility? The simplest picture of the low field mobility treats the scattering processes with a single scattering rate; electrons are accelerated by the electric field until they are scattered, after which they start with zero velocity again. For a scattering rate of $1/\tau$, the fraction of electrons which have not scattered decays exponentially with time constant τ. The average velocity of electrons in an electric field E can then be calculated by computing expectation values of the mean free path and mean free time in this distribution, giving a mobility of $e\tau/m^*$. This is the same obtained from the full solution of the Boltzmann transport equation in the relaxation time approximation. For the warm electron case, we can imagine a situation wherein the electron is scattered at a rate of $1/\tau$ until it reaches some critical energy, and then immediately scatters.[i] For phonon emission, this critical energy would be $\hbar\omega_{LO}$, and an un-scattered (ballistic) electron would reach the critical energy and emit a phonon in $\tau_{LO}=\sqrt{2m^*\hbar\omega_{LO}}/(eE)$ seconds. Doing the same type of calculation for the expected value of the mean free path and time as used for the single scattering rate model, the mobility is

$$\mu = \frac{e\tau}{m^*} \frac{1 - (x^2/2 + x + 1)\, e^{-x}}{1 - (1 + x)\, e^{-x}} \qquad (17)$$

where $x = \tau_{LO}/\tau$. A log-derivative plot of the current-field characteristic for such a model is shown as a solid line in figure 27. This model reproduces the general shape of the experimental data better than than the warm-electron coefficient expression, but cannot fit the low and high field behavior simultaneously. If we assume that optical phonon emission is the dominant process reducing the mobility at high field, we can use the fitted parameters in equation (17) to give a measure of τ, and the corresponding mobility. For

[i] This sort of approach is in the spirit of the "lucky electron" model used by Shockley for hot electrons.

the fit of the data from figure 10 we get a low field mobility of 25,200 cm^2/Vs, which is in reasonable agreement with the mobility expected for the temperature of the measurement. One can modify the model to give any desired behavior throughout all ranges of electric field. For example, we can consider a "two scattering rate model", which is similar to the abrupt emission model, except that it assumes a second, finite scattering rate for electrons which have gone un-scattered longer than τ_{LO}. For this model, the mobility is given by

$$\mu = \frac{e^2\tau}{m^*} \frac{1 - e^{-x}(1 - x(1-y) - y^2)}{1 - e^{-x}(1 - y)} \qquad (18)$$

where now $y = \tau'/\tau$; $1/\tau'$ is the second scattering rate. The grey curve in figure 27 uses y=2.6, and a low energy scattering rate corresponding to a mobility of 41,100cm^2/Vs to fit the data from figure 10. Note in figure 27 that while the low field behavior of the two-rate model is identical to the abrupt emission model, at high fields, a plateau in the conductivity exponent is observed. This is easy to understand by considering that at very high fields, the low energy scattering rate will be unimportant, and a return to ohmic behavior (and a logarithmic derivative of 1) is expected. A different choice of τ'/τ will change the level and slope of the plateau seen in figure 27. One can imagine more complicated models with multiple scattering rates to better match the observed current-field characteristics. One more such model, in which the scattering rate for energies above the phonon energy is assumed to rise linearly, is also shown as the dotted curve in figure 27.

The point of these models is not so much to provide a glove-tight fit to the data as it is to provide some help interpreting the current vs. field data. They allow extraction of the mobility from current-field data without requiring any knowledge of the carrier density, or of the sample size. The rough agreement of these extracted mobilities with Hall mobilities measured on larger samples is a good indication that the interpretation of the non-ohmic behavior in terms of electron heating and phonon emission is reasonable. It would be a mistake, however, to take these models too literally. Since the models are one dimensional, they ignore the effects of momentum perpendicular to the electric field. In a three-dimensional system,

the existence of perpendicular momentum will allow phonon emission to occur even with zero parallel momentum. To model this in one dimension would require a scattering rate which changed gradually as a function of energy, even in the case where phonon emission was absolutely abrupt.

The second drop-off of the conductivity exponent at higher fields is not predicted by any of the models described here. To fit this second drop-off in a similar model would require a second energy range of sharply increased scattering. This would require a scattering process other than the phonon emission process observed at the relatively low fields. It is well known that as electrons in GaAs are heated to energies above the L-valley minimum, they are quickly scattered to these L-valleys. The large effective mass in the L valleys then gives rise to reduced mobility and consequently, the Gunn effect. The electric field at which the drop-off occurs is consistent with this interpretation. Since the conduction in this field range depends on the relative populations of the L and Γ valleys rather than on scattering rates, it does not make sense to extend the sort of model discussed above to this field region. There are other difficulties in the interpretation of this high field data. For currents slightly higher than those used for these measurements, appreciable substrate current begins to flow. It should be no surprise that these two effects occur at close to the same current levels, since fields which allow significant valley transfer, and thus negative differential resistance, are inherently unstable. The possibility of substrate current also suggests a different explanation for the high field data: back-gating. Electrons injected and trapped in the substrate may change the interface depletion in the epitaxial layer, thus reducing the carrier density. This may explain the large spread in the measured logarithmic derivatives at high field shown in figure 15. In either case, the high field drop-off in the logarithmic derivative can be interpreted as a direct or indirect consequence of the valley transfer of electrons in the epitaxial layer.

As seen in figure 15, the high field current-field behavior seems to be modified by the application of magnetic fields. The plateau in the conductivity exponent of the current-field curves appears to extend well beyond 1kV/cm. (The low field behavior will be discussed below.) The origin of this magnetic field effect is unclear. One possibility is that this is a result of the phenomenon for which this experiment was searching, the formation of polaron gaps in magnetic fields. As discussed in Chapter 2, the

one dimensional confinement of the electrons in a magnetic field can give rise to large energy shifts for electrons with nearly the phonon energy. These shifts open an energy gap between zero-phonon states above and below the phonon energy, giving rise to an enhancement of the phonon emission rate for electrons with exactly the phonon energy. In moderate electric fields parallel to the magnetic field, this could give rise to enhanced cooling of the electrons, and thus a suppression of processes such as valley transfer which appear to cause the sharp decrease of the conductivity exponent for zero magnetic field. An enhancement of the phonon emission process might also be expected to show up in the initial fall-off of the conductivity exponent below 100V/cm. No dramatic effect is observed in this region, but the superlinearity at low electric fields might be expected to mask these effects. Although it seems surprising that such a small gap (0–5meV, depending on the wave vector) would remain significant at temperatures above liquid nitrogen ($kT \approx 7meV$), the details of how these wave vector dependent gaps would affect transport have yet to be worked out. If polaron gaps are the explanation for the sharp decrease of the conductivity exponent, then the lack of these decreases at 4K would suggest that the polaron cusp predicted for 3-dimensions has a larger effect on transport than previously thought.

A second possible explanation for the magnetic field effect is based on the presumption that back-gating effects are directly responsible for the high field drop-off in conductivity exponent. If this was true, then the effect of a parallel magnetic field might be simply to suppress injection of electrons into the substrate, perpendicular to the magnetic field. This effect should not be present when the magnetic field is oriented normal to the substrate. The absence of a conductivity exponent drop-off in figure 17 would thus argue against this explanation.

A third explanation is based on the coincidence of low field superlinear behavior and the extended high field sublinear plateaus. If the low-field superlinear behavior is due to ionization of neutral donors, as discussed below, then at higher fields inelastic scattering by the neutral donors may enhance the electron cooling, thus suppressing valley transfer just as for the case of the polaron gap. Although this idea has the appeal of unifying the low and high field behaviors, neutral donors appear to be ionized at low fields, and thus are not available to provide inelastic scattering at high fields.

In summary, the high electric field measurements clearly show the

effects of phonon emission. The observation of changes in the conductivity exponent with magnetic field provides support for the existence of polaron gaps in large magnetic fields. However, alternate explanations for this effect must be seriously considered.

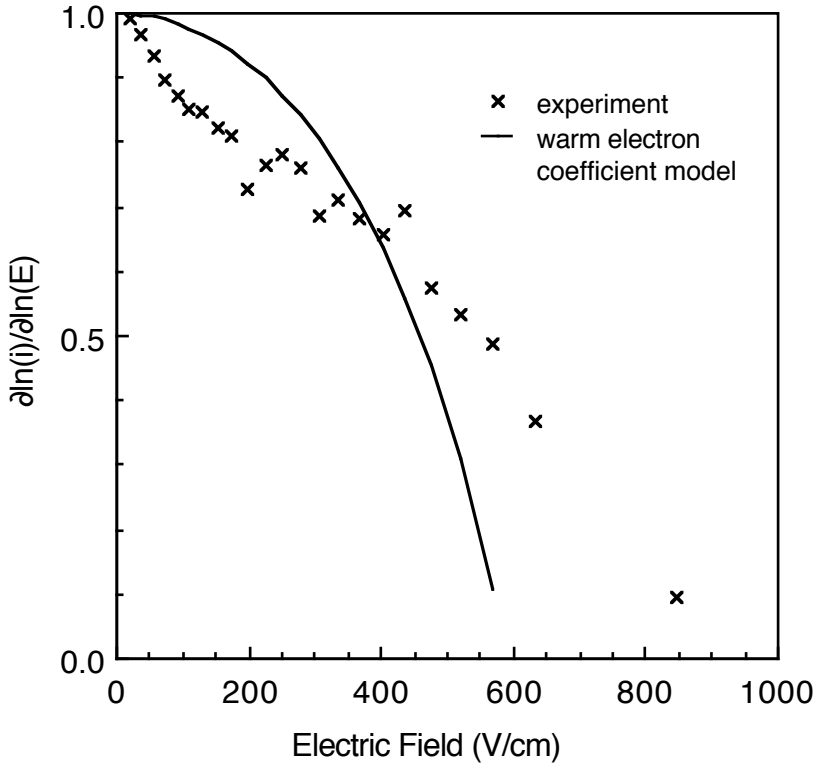

Figure 26. Comparison of experimental data with the warm electron expansion $\mu = \mu_0(1+\beta E^2)$ with $\beta=(1/5.134\text{V})^2$ fit to the data.

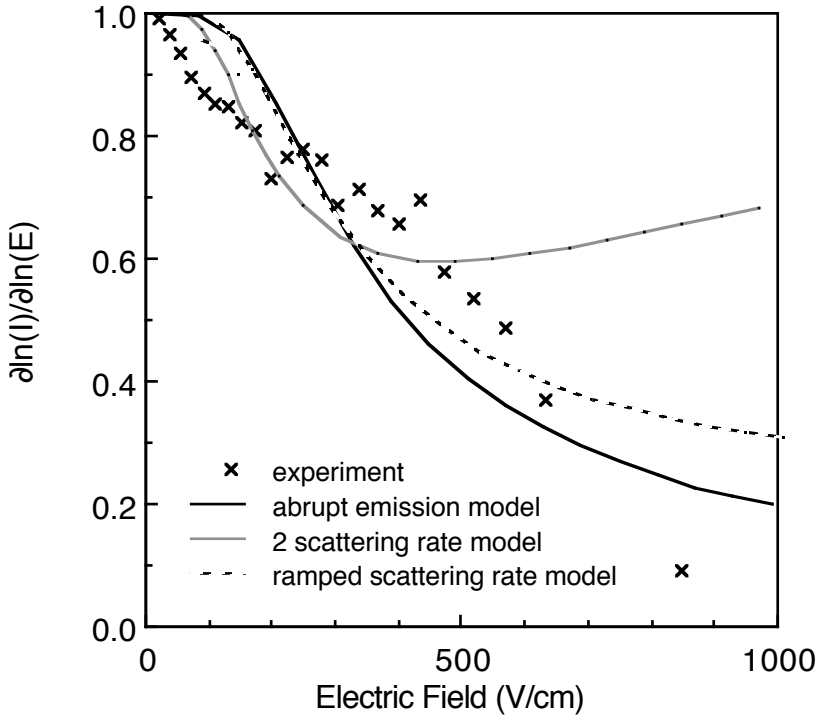

Figure 27. Comparison of experimental data with three models for the mobility described in the text. The abrupt scattering model assumes a single scattering rate until the electron reaches the phonon energy, whereupon it immediately scatters. The two scattering rate model assumes different scattering rates above and below the phonon energy. The ramped rate model assumes a linearly increasing scattering rate above the phonon energy. For each model, parameters have been chosen to give a best fit to the current-field data. The conductivity exponent plot accentuates the differences between theory and experiment.

4.5.2 Freeze-Out and Impact Ionization

The importance of impact ionization of neutral impurities for low temperature transport in high purity semiconductors has been known since the late 50's from work on p-type Ge.[72] Superlinear current-voltage characteristics due to impact ionization of donors in GaAs were widely studied following the work of Oliver.[73] These effects are observed only in material with impurity densities low enough that the conductivity through impurity bands is small, and only at temperatures where the electrons are frozen onto the shallow impurity levels. The current-field characteristics for such samples generally show a sharp turn on behavior at some critical field, where the donors become ionized. In closely compensated material, the current-field curve can even be S-shaped, resulting in current controlled negative differential resistance. The present experimental results shown in

figure 18,19 and 20 correspond closely to this previous work.

The phenomenon of magnetic freeze-out was discussed in Section 3.2, and the observed increase of low field resistivity with increasing magnetic field was discussed in Section 4.4. The interaction of magnetic freeze-out and impact ionization was studied in some depth by Poehler,[74] who measured current-field characteristics of GaAs epitaxial films at low temperatures in magnetic fields of up to 4.1T. He observed that the critical fields for impact ionization approximately doubled with a 4.1T magnetic field normal to his sample. Poehler used models for the impact ionization rates to extract donor binding energies as a function of magnetic field. He obtained binding energies significantly lower than predicted by Yafet, Keyes and Adams,[37] and he attributed these differences to disorder broadening of the conduction band. Although the carrier concentrations in his films were the same as used in the present work, his total impurity concentration was more than 5 times higher. Poehler reported very little change in the critical fields for magnetic fields applied parallel to the current flow.

The 4K experimental results described in Section 4.4 are similar to those reported by Poehler. The impact ionization is observed as a low field superlinearity in the current-field curves. While the critical field for impact ionization, taken to be 4V/cm in figure 20, is similar to Poehler's, no negative differential resistance is observed, consistent with the higher purity of the material used in this work. The electric fields measured for the present work extend almost 2 orders of magnitude higher than those used by Poehler. As seen in figure 19, the superlinearity at 4K persists up to about 50V/cm. This suggests that processes involving the neutral donors continue to affect the transport at fields well above the the onset of impact ionization.

The population of neutral donors during impact ionization is determined by a balance between ionization and capture processes. Since both impact ionization and capture processes (other than Auger processes) are linear in the carrier density, the fraction of neutral donors (in the absence of compensation) can be expressed as a simple ratio of rate constants:

$$\frac{N_D^0}{N_D} = \frac{R_C}{R_I + R_C} \qquad (19)$$

where R_C and R_I are the linear capture and ionization rate coefficients, respectively. The turn-on of the conductivity at a critical field can thus be interpreted as a sharp increase in the impact ionization rate due to heating of the electrons above the donor ionization energy. The weak superlinearity up to 50V/cm means that either the ionization rate continues to increase with increasing field, or that the capture rate decreases with increasing field. Both of these effects probably occur, but detailed calculations of their relative magnitudes have not been done.

The superlinear conductivity exponents measured in magnetic fields near 80K, seen in figures 14 and 17, are quite surprising. The superlinearity for transport normal to 7T extends to fields well above 500V/cm, an order of magnitude higher than at 4K without magnetic field, while in parallel magnetic field, weak superlinearity is seen up to 100V/cm. It is reasonable to assume that this superlinearity is related to the magnetic freeze-out observed in the low field conductivity, and has the same origin as the weak superlinearity below 100V/cm associated with impact ionization at 4K. While the parallel field data can be reasonably accounted for by the magnetic deepening of the donor, the strong enhancement of the superlinearity in perpendicular magnetic field must have a different origin. In any case, the data show that the ionization/capture balance is strongly affected by the orientation of a magnetic field relative to the electric field. The exponent drop-off associated with phonon emission also appears shifted to higher field in perpendicular magnetic fields, indicating that the magnetic fields are effective in suppressing carrier heating.

The poor reproducibility of the measurements in the superlinear range is consistent with the mechanism of impact ionization. It has been demonstrated experimentally that large noise levels are a signature of impact ionization[75], and that the current flow is unstable with respect to filimentation.[72].

4.5.3 Oscillatory Magneto-Resistance

The structure observed in the magnetic field sweeps of the magneto-resistance appears to be closely related to a phenomenon known as the magneto-impurity resonance effect. This topic was reviewed by Eaves and Portal[76] in 1978. The phenomenon arises from inelastic scattering which

occurs when the separation between Landau levels becomes equal to an excitation energy of a shallow impurity level. The resonant scattering can be seen as very sharp structure, periodic in 1/H, when the resistivity is differentiated with respect to the magnetic field. Magneto-impurity resonances have been observed in n-GaAs, n-InP, p-Te, n-Ge and p-Ge, and a variety of different impurity excitation energies have been observed. Phonon structure is also observed in some measurements. Observation of these effects requires hot carrier excitation, either by photo-excitation or by electric fields large enough to get non-ohmic (warm-electron) conduction. Very high purity material is also necessary for observation of the effects. Most of the observed effects have been too small to be seen except in derivative spectra. In the case of InP, Nicholas and Stradling[77] observed a resonance corresponding to the transition between the 1s ground state of the impurity and the conduction band which was intense enough to "be observed directly in the magnetoresistance without resorting to derivative techniques."[76] The largest magnitude resonances were reported by Zverev and Shovkun[78] for GaAs excited by infrared radiation.

Magneto resistance oscillations, periodic in 1/H, are also characteristic of the magneto-phonon effect[79]. This phenomenon involves resonances between the cyclotron energy and the phonon energy. The two magnetophonon series which are usually seen in in GaAs are the LO phonon series, with fundamental at 21T, and the 2 TA(X) phonon series, which involves emission of pairs of band edge phonons, with fundamental at 11.4T. At low temperatures, these oscillations shift to higher fields by an amount corresponding to the donor binding energy, so that the resulting effect is a combined magnetophonon and magneto-impurity effect. The magneto-impurity resonances which have been observed in GaAs are the 1s to $2p^-$ hydrogenic impurity transitions which come at fields lower than the fundamental at 2.4T. The 1s to conduction band transitions have been observed for InP[80], but they have been mysteriously absent in the measurements on GaAs.[76]

In comparison to the previous work on the magneto-impurity resonance effect, the magnetoresistance structure reported here is very broad and huge in magnitude, comparable only to the oscillations in photo-excited GaAs

reported by Zverev and Shovkun.[j] Oscillations periodic in 1/H are not observed. Since the electron concentration of the samples is significantly larger than for any previous magneto-impurity experiment, the breadth of the peaks is not surprising, and may wash out 1/H oscillations below the fundamental. The dependence of the position and amplitude of the the peaks and dips seen in figures 22, 23, 24 and 25 on measuring conditions and field orientation is rather complicated, but similar to what has been previously reported. The occupation of the shallow donors and their excited states depends critically on the electron temperature and field strength. For low electron temperatures, it is expected that the inelastic process with the smallest energy should be most important. This should be the $1s–2p^-$ transition for the GaAs neutral donors. The sharp dip in magneto-resistance at 2.4T seen in the low current sweep shown in figure 25 is almost certainly a resonance with this transition. The broad dips between 4.5T and 5T in the longitudinal magnetoresistance data can be attributed to resonances of the cyclotron energy with the donor binding energy. Calculations of the dependence of the donor binding energy[81] on magnetic field indicate that this resonance should actually occur at a slightly higher field. This calculation is shown in figure 28, along with the cyclotron energy. Since the dips seen in all the present data are very broad, it seems reasonable that the dips between 4.5T and 5T correspond to resonances with bands of shallow excited states of the impurity which lie at fields just below the full ionization. Previous experiments would have resolved this dip into separate sharp structures in the 2nd derivative of the magnetoresistance. The peak at 5.2T in the perpendicular magnetoresistance , figure 24, is probably also the donor ionization resonance. Since current flows by scattering in perpendicular fields, conversion of the resonance from a dip to a peak is not surprising. Similar peak inversions have been seen previously.[76] The peak at 3.3T in the same plot might be due to the 1s to $2p^0$ transition. It is not clear why this transition should be seen instead of the 1s to $2p^-$ transition seen at lower current.

The structure observed at higher magnetic fields is quite a bit more puzzling. In figure 22 it appears that another minimum centered between 9T

[j] The measurements by Zverev and Shovkun are also the only other magneto-impurity measurements on GaAs done at 4K.

and 10T would come just above the high field limit of our measurements. Structure between 8 and 9T also is seen in figures 23 and 24. In previous work, all of the magnetoresistance structure above the magneto-impurity resonances has been attributed to magnetophonon resonances. However, neither the LO phonon nor the TA phonon pair magnetophonon series can be fit to the data, even if impurity shifts are taken into account. Pair excitations (ionization or excitation of two neighboring neutral donors by impact of a single electron) could produce peaks at the right fields, but only if 1s to $2p^-$ transitions are paired with higher excitations. For an impurity density of $1x10^{15}/cm^3$, the mean nearest neighbor distance between impurities is 440Å, which implies that inter-donor coupling could occur for a significant fraction of the impurities. However, since the fundamental 1s to $2p^-$ transition at 2.4T is not seen in figure 22, it seems unlikely that pair excitation involving this excitation should be so important. The most likely possibility is that this magnetoresistance dip is related to a resonance between the donor binding energy and the X-edge TA phonon energy which occurs at 8.4T. This would be the first observation of this magneto-impurity-phonon resonance effect.

The large magnitude of the oscillations observed in this study are both unusual and significant. No theoretical estimates have been made of the expected magnitude of this effect, and in view of the complicated dependence of the amplitude on measuring conditions, none are forth-coming. The fact that the Soviet experimenters using photo-excitation observed effects of similar magnitude for similar carrier densities and helium temperatures suggests that these conditions are important factors in the magnitude of the effect. Still, the observation of donor ionization effects at current densities greater than $10A/cm^2$ and in electric fields higher 200 V/cm allows us a significant insight into the transport properties of warm electrons in GaAs.

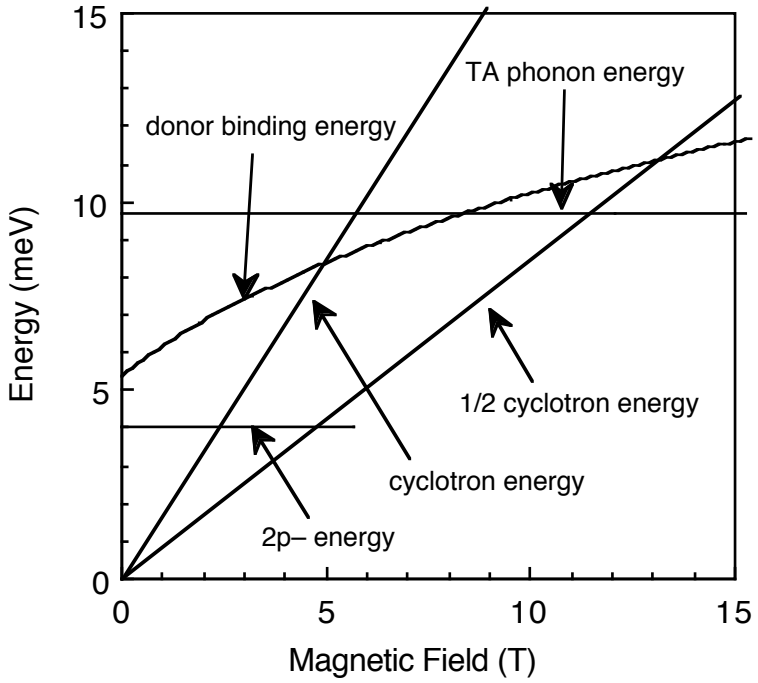

Figure 28. Calculated donor binding energy from reference 81 and cyclotron energy plotted as a function of magnetic field. Resonant impact ionization can occur when these curves cross at about 4.9T. Also shown are the TA phonon energy and the energy of the $2p^-$ donor excited state.

5. Conclusions

5.1 Heterojunction Tunneling The observation of phonon structure in heterojunction tunneling experiments provides specific information about the role of optical phonon emission in the magnetotransport properties of lightly doped GaAs, as discussed in Chapter 3. The presence of a tunnel barrier allows the hot electron distribution to be controlled external to the high purity GaAs layer. Similarly, the observation of impact ionization and other effects in experiments on bulk materials allows us to separate effects intrinsic to the tunneling process from bulk effects in the tunneling experiments. In addition, the magnitude of the observed effects can in each case provide information about which effects are likely to be important in the other.

5.1.1 Impact vs. Phonon Ionization

Since the magneto-impurity effect and possibly a magneto-phonon-impurity effect are seen clearly in the magnetic field sweeps of the longitudinal magneto-resistance of GaAs, the measurements of bulk properties might be expected to provide insight into the controversy over whether impact ionization or phonon ionization is the primary mechanism for the influence of phonon emission on space charge in the lightly doped GaAs layers of the tunneling structures studied by the IBM and Nottingham groups. While impact ionization has generally been accepted as the important process leading to superlinear current voltage characteristics of GaAs at low temperatures, the process of phonon ionization was not considered before Leburton proposed it as a mechanism in the heterojunction devices. This is because the phonon ionization process requires much hotter electron temperatures than impact ionization. The superlinear current voltage behavior begins at electric fields much too small to generate the energetic electrons required for phonon emission to become important, thus ruling out phonon ionization as the primary mechanism. However, hot electrons are injected directly into the lightly doped layer by the very large fields in the heterostructures, and thus phonon ionization cannot be ruled out as an important mechanism.

The observation by the Nottingham group of a magneto-impurity like

effect in the dependence on magnetic field of the LO-phonon oscillation amplitude seems to confirm the role of impact ionization in the tunneling experiments. Although resonances of the donor ionization with the cyclotron energy at 5.1T (as opposed to the donor excitation at 2.4T) had not been previously observed in bulk measurements, the present work confirms that this resonance does indeed occur and even dominates the transport at large current densities and electric fields. Why then is there no enhancement of the oscillations at the same magnetic field in the data of Hickmott et. al.? One possibility is that impact ionization is not the dominant ionization mechanism for the very low current densities in the devices used by Hickmott et. al.. This conclusion is supported strongly by the results of bulk resistivity measurements. The threshold current density for impact ionization measured in the present experiments is far above the current density in the Hickmott devices. Also, the very sharp increase, and sometimes negative resistance, observed in the current-voltage curves at the threshold of impact ionization must be caused by an increasing dependence of the impact ionization coefficient on the current density. This is usually explained as being due to a 2-step ionization process. Presumably, phonon ionization might then be the dominant ionization mechanism at very low current density. To prove this, one might look for a magneto-phonon-impurity resonance in the heterostructure tunneling data, similar to that observed in the present bulk data. This should occur at about 53T (where $2E_D(H)= E_{LO}$), or lower if conduction band non-parabolicity is taken into account.

Coherence is still a problem with the impact ionization explanation. Can the impact ionization rate be so sensitive to the electron energy that even when most of the electrons are many phonon energies above the donor binding energy, as they are at high bias voltages in the tunneling experiments,[60] the space charge of ionized impurities still shows oscillations with the periodicity of the phonon energy? The bulk measurements show that superlinear behavior characteristic of donor ionization persists even at high fields and high current densities, suggesting that the balance of neutral and ionized donors might be crucial even in the hot electron regime. The dependence of the impact ionization cross-section on incident electron energy was calculated for application to atomic hydrogen,[82] and depends critically on electron energy only near the threshold. However, the equation for the neutral donor density, equation (19), also contains a capture term

whose dependence on the low energy electron distribution may account for the observed coherence of the oscillations. Another possibility is that the impact ionization probabilities are significantly altered by application of magnetic fields. This possibility is considered in Appendix 2.

5.1.2 Current Inhomogeneity

The observation of current-controlled negative differential resistance in bulk low-temperature measurements of closely compensated GaAs suggests a very natural mechanism which might lead to inhomogeneous current flow in the heterojunction tunneling experiments. Current flow in materials with current-controlled negative differential resistance is inherently unstable with respect to current filimentation.[69] Since a tunnel barrier also has a highly nonlinear conductance, it would accentuate any current inhomogeneity originating in the lightly doped layer. Thus, models of heterojunction tunneling which consider donor ionization to be important should consider seriously the window model of Hanna et. al..[38] A simple way to test the importance of current inhomogeneity induced by impact ionization would be to measure the amplitude of phonon oscillations in a set of samples with constant impurity density, but different degrees of compensation. If current inhomogeneity is important, the most compensated samples should show the largest amplitude phonon oscillations.

5.1.3 Freeze-out

The role of freeze-out and magnetic freeze-out in the tunneling experiments is substantially clarified by examination of the bulk measurements. At 4K, lightly doped GaAs of the same carrier concentration used in the tunneling experiments and of reasonably low compensation exhibits carrier freeze-out even without magnetic fields. At 80K, magnetic fields of 4.5T are enough to cause some freeze-out, as evidenced by superlinear current voltage characteristics, and increased resistivities. The notion expressed by Hickmott et. al.[26] that the capacitance-voltage measurements give directly the free carrier concentration is thus seen to be flawed. Their claim that all the donors remain neutral under magnetic freeze-out conditions is also contradicted by the bulk measurements of the resistivity during the magnetic field sweeps.

The explanation by Eaves et. al.[40] for the absence of phonon oscillations without magnetic fields in the data of Hickmott et. al. is consistent

with the bulk measurements. At the small current densities of those experiments, the conductivity of the lightly doped layer due to impurity hopping is probably high enough to prevent significant voltage drops across it. The stronger localization of the bound electrons in a quantizing magnetic field can reduce this conductivity drastically.

5.2 Pinned Polarons?

The experimental work on phonon structure in heterojunction tunneling and on parallel magneto-transport of hot electrons has so far given little support for the existence of the one dimensional pinned polarons discussed in Chapter 2. The phonon oscillations appear to be related to ionization of neutral donors in lightly doped layers of the tunneling device, although enhancement of phonon emission by polaron gaps could possibly play a role in the remarkable persistence of the oscillations at voltages corresponding to tens of phonon emissions. The high field current-field characteristics of thick films show evidence for enhanced cooling in the presence of quantizing magnetic fields, and while a polaron gap is a definite possibility, other mechanisms appear to be equally likely.

To find unambiguous effects of the polaron pinning in magnetic fields will probably require more elaborate experiments than those discussed here. One type of experiment would involve more direct methods of measuring drift velocities of mono-energetic electrons. This approach would avoid the problems caused by inter-valley scattering by injecting electrons well below the subsidiary valley minimum. The experiment could essentially be a time resolved version of the oscillatory photoconductivity experiments.[47] Alternatively, one can imagine doing hot electron spectroscopy[83] with barriers on the phonon energy scale to study transport properties of pinned polarons.

In general, though, it is hard to distinguish the properties of a pinned polaron from a low energy free electron in the presence of an uncorrelated LO phonon. The distinguishing characteristic is the binding of the electron to the phonon and the resulting negative effective mass. This characteristic suggests another possible way to observe pinned polarons. The negative effective mass should lead to a negative electrical conductivity. Thus if the pinned polarons were produced in sufficient densities, they might give rise to observable amplification of AC electric fields.

Postscript

The heterojunction tunneling work of Hickmott et. al. has been a fresh, clean rediscovery of the point-contact and oscillatory photoconductivity work of the late 60's and early 70's, which, as pointed out by Lu et. al., was a solid-state re-invention of the Franck-Hertz experiment[k] of the 1910's.[84] The theorists have responded to the renewed challenge with fresh, invigorated re-inventions of old theories (which were, in turn, re-interpretations of older theories). The elimination of dirt, grime and surface oxides from the experiments has allowed the theory to probe deeper into the physics hidden in the data. (Theories, by design, are free of dirt and grime.)

The polaron problem was invented and solved in the 50's. Its pathologies were recognized in the 60's, and the less virulent ones cured in the 70's. It was bold of me to tackle the divergences of the one-dimensional polaron problem but even more bold to think that it might matter. The experiments indicate that they probably don't matter much……yet.

---

[k] In this experiment, the impact ionization energy of mercury atoms was determined by accelerating electrons through mercury vapor. When the accelerating voltage was equal to the ionization energy divided by the electron charge, the current was reduced.

Appendix 1: Variational Calculation of the Energy-Momentum Relation For a Polaron in a Strong Magnetic Field.

The wavefunctions for free electrons in a magnetic field **H**=H ✽✽▮ in the Landau gauge are:[13]

$$|k_x,k_z,m\rangle = \frac{1}{\Omega^{1/3}C_m} e^{ik_x x + ik_z z} e^{-Y^2/2} H_m(Y) \qquad (20)$$

where Ω is the system volume, the normalization factors are $C_m=(2^m m!\sqrt{\pi}$ $L)^{-1/2}$ the center of the wavefunction in the ◊ direction is at

$$Y = \frac{y - k_x L^2}{L} \qquad (21)$$

the magnetic confinement length is

$$L=\sqrt{\frac{\hbar c}{eH}} \qquad (22)$$

and the $H_m(x)$ are the Hermite polynomials. These are energy eigenstates of the electron Hamiltonian with eigenvalues

$$E_{k_x,k_z,m} = \frac{\hbar^2 k_z}{2} + (m+1/2)\hbar\omega_c \qquad (23)$$

where

$$\hbar\omega_c = \frac{eH}{m^* c} \qquad (24)$$

is the cyclotron frequency.

The electron-phonon interaction is treated using the Fröhlich Hamiltonian,which is usually written with the electron in first quantization,

$$H_{e\text{-}\varphi} = \sum_{\mathbf{q}} V_q e^{-i\mathbf{q}\cdot\mathbf{r}} \; (a^{\dagger}_{\mathbf{q}} + a_{-\mathbf{q}}) \tag{25}$$

where

$$V_q = \hbar\omega_{LO} \sqrt{\frac{4\pi\alpha}{\Omega\, k_{LO}}}\; \frac{1}{q} \tag{26}$$

and α is the dimensionless coupling constant:

$$\alpha = \frac{m^* e^2}{\hbar^2 k_{LO} (\varepsilon_\infty^{-1} - \varepsilon_0^{-1}) - 1} \tag{27}$$

and $k_{LO} = \sqrt{2m^*\omega_{LO}/\hbar}$ is the wave vector of an electron with energy $\hbar\omega_{LO}$. The electrons have wave vectors $\mathbf{r}$, while the phonons, with wave vectors $\mathbf{q}$, have the creation and destruction operators $a^{\dagger}_{\mathbf{q}}$ and $a_{\mathbf{q}}$, respectively. With no magnetic field, the electron states are plane waves and each term in this Hamiltonian couples each electron state to one other electron state. With magnetic fields, each phonon couples every electron state to one electron state in each Landau level. This coupling can be written in second quantization by using the electron creation and annihilation operators $c^{\dagger}_{k_x,k_z,m}$ and $c_{k_x,k_z,m}$ as follows:

$$H_{e\text{-}\varphi} = \sum_{m,m'} \sum_{\mathbf{q}} V_q \sum_{k_x,k_z} M^{mm'}_{\mathbf{k},\mathbf{q}} \; c^{\dagger}_{k_x - q_x, k_z - q_z, m} \; c_{k_x,k_z,m'} \; (a^{\dagger}_{\mathbf{q}} + a_{-\mathbf{q}}) \tag{28}$$

$M^{mm'}_{\mathbf{k},\mathbf{q}}$ are defined as matrix elements of the plane wave between the Landau states:

$$M^{mm'}_{\mathbf{k},\mathbf{q}} \equiv \langle k_x - q_x, k_z - q_z, m | \; e^{-i\mathbf{q}\cdot\mathbf{r}} \; | k_x, k_z, m' \rangle \tag{29}$$

We will only be interested in the lowest Landau level, so the matrix element is evaluated as

$$M^{00}_{\mathbf{k},\mathbf{q}} = e^{-iq_xq_yL^2/2}\, e^{ik_xq_yL^2}\, e^{-q_\perp{}^2L^2/4} \qquad (30)$$

where $q_\perp{}^2 = q_x{}^2+q_y{}^2$ is the component of the phonon wave vector perpendicular to the magnetic field. The corresponding matrix element for the one-dimensional parabolic potential given by equation (11) is the same, but with out the phase factor $e^{ik_xq_yL^2}$.

An accurate calculation of polaron energies in a magnetic field which approach the phonon energy is difficult because of divergent integrals and has not been done previously. The k_Z=0 energy and effective mass for polarons in a magnetic field has been calculated by variational techniques and applied to cyclotron resonance measurements.[85,86,24] The Fröhlich Hamiltonian couples states in one Landau level to states in all Landau levels, making an exact calculation of energy shifts difficult. However, in strong magnetic fields the contribution of Landau levels other than the lowest will be small. If we choose a trial wavefunction composed only of electrons in the lowest Landau level, the problem is reduced to one in which the electron is effectively one dimensional. Although this will result in a poor value for the ground state energy shift for small magnetic fields such that $\hbar\omega_c$ is not much greater than $\alpha\hbar\omega_{LO}$, the true energy must be lower than that which is calculated.

The quasi-one dimensional polaron problem is still complicated for energies near the phonon energy because an accurate description of the polaron wavefunction must include contributions from two phonon states, since almost enough energy exists to create one real phonon. Since a Wigner-Brillouin calculation can include only one phonon, the energy shifts it would give for energies near the phonon energy do not reflect the shift of the ground state energy. To include more than one phonon in the calculation, I have chosen to extend a variational method given by Larsen [20,24] but first used by Haga [87] for three dimensional polarons. The strategy is to solve the variational problem in two steps. First, build a variational wavefunction to describe the polaron at k_Z=0, then add in an extra phonon to describe the behavior for higher energies.

An analog of the unitary linear shift operator introduced by Low, Lee and Pines,[88]

$$U_{LS} = \exp\Big[\sum_{\mathbf{q}} f_{\mathbf{q}} g_{\mathbf{q}} \, (a_{\mathbf{q}}^{\dagger} - a_{-\mathbf{q}})\Big] \tag{31}$$

is used to solve the k_z=0 problem. Here $f_{\mathbf{q}}$ is defined as a unitary operator

$$f_{\mathbf{q}} \equiv \sum_{m} \sum_{k_x,k_z} c^{\dagger}_{k_x-q_x,k_z-q_z,m} \qquad c_{k_x,k_z,m} \tag{32}$$

which takes the x and z components of the momentum $\mathbf{q}$ from the electron and preserves Landau level. The symmetry $g_{-\mathbf{q}} \equiv g_{\mathbf{q}}$ is also built in. The trial wavefunction for k_z=0 is then $U_{LS} c^{\dagger}_{k_x,0,0} \, |0\rangle$, and we use the real scalars $g_{\mathbf{q}}$ as variational parameters. Although this wavefunction includes many-phonon states, we have chosen to use it because it facilitates the addition of an independently variable phonon. Since U_{LS} is unitary, the algebra involved in adding the additional phonon is considerably simplified compared to trial wavefunctions which contain only zero- and one-phonon states. The ground state energy can be evaluated as the expectation value of a transformed Hamiltonian $\tilde{H} \equiv U_{LS}^{-1} H U_{LS}$ in the one-electron k_z=0 non-interacting ground state. Using the simple transformation properties $U_{LS}^{-1} f_{\mathbf{q}} U_{LS} = f_{\mathbf{q}}$ and $U_{LS}^{-1} a_{\mathbf{q}} U_{LS} = a_{\mathbf{q}} + g_{\mathbf{q}} f_{\mathbf{q}}$, we find the transformed non-interacting Hamiltonian to be:

$$\tilde{H}_0 = \frac{\hbar^2}{2m^*} \Big\{ \sum_{k_x,k_z,m} k_z^2 \, c^{\dagger}_{k_x,k_z,m} \qquad c_{k_x,k_z,m} \qquad + \sum_{\mathbf{q}} |$$

$g_{\mathbf{q}}|^2 \, q_z^2$

$$+ \sum_{\mathbf{q}} g_{\mathbf{q}} (a^{\dagger}_{\mathbf{q}} - a_{-\mathbf{q}}) \Big(q_z^2 f_{\mathbf{q}} - 2 q_z \sum_{k_x,k_z,m} k_z$$

$c^{\dagger}_{k_x-q_x,k_z-q_z,m} \qquad\qquad c_{k_x,k_z,m} \qquad \Big)$

$$+ \sum_{\mathbf{q}\mathbf{q}'} q_z q'_z f_{\mathbf{q}+\mathbf{q}'} g_{\mathbf{q}} g_{\mathbf{q}'} \left(a_{\mathbf{q}}^{\dagger} a_{\mathbf{q}'}^{\dagger} + a_{-\mathbf{q}} a_{-\mathbf{q}'} - 2a_{\mathbf{q}'}^{\dagger} a_{-\mathbf{q}}\right)\Big\}$$

$$+ \hbar\omega_c \sum_{k_x,k_z,m} (m+\tfrac{1}{2}) c^{\dagger}_{k_x,k_z,m} c_{k_x,k_z,m}$$

$$+ \hbar\omega_{LO} \sum_{\mathbf{q}} \left(a_{\mathbf{q}}^{\dagger} a_{\mathbf{q}} + f_{\mathbf{q}} g_{\mathbf{q}} (a_{\mathbf{q}}^{\dagger} + a_{-\mathbf{q}}) + |g_{\mathbf{q}}|^2\right) . \qquad (33)$$

A single electron is assumed, so two electron terms drop out and $f_0=1$. The transformation of the interaction Hamiltonian is more complicated because the operator $\sum_{k_x,k_z} e^{ik_x q_y L^2} c^{\dagger}_{k_x-q_x,k_z-q_z,m} c_{k_x,k_z,m'}$ does not have convenient transformation properties. However, in certain situations, the entire phase $e^{ik_x q_y L^2}$ $e^{iq_x q_y L^2/2}$ can be replaced by one, and then the interaction Hamiltonian can be easily transformed. If this is done, and only states which have one electron in the lowest Landau level are considered, equations (28),(34), and (31) can be used to find the transformed interaction Hamiltonian

$$\mathcal{H}_{e\text{-}\varphi} = \sum_{\mathbf{q}} V_q e^{-q_\perp^2 L^2/4} \Big(\sum_{k_x,k_z} c^{\dagger}_{k_x-q_x,k_z-q_z,0} c_{k_x,k_z,0} \left(a_{\mathbf{q}}^{\dagger} + a_{-\mathbf{q}}\right) + 2 g_{\mathbf{q}} \Big) \qquad (35)$$

Since this Hamiltonian is used to calculate the energies of variational states, setting the phase to one is equivalent to adjusting the phases of each part of the trial wavefunction so that this phase in the interaction is canceled. Such an adjustment is possible for the one-phonon parts of the trial wavefunction because the phase drops out of the non-interacting Hamiltonian. Once the phases of the one-phonon parts are set, it is not possible to completely cancel the phase for two or more phonon parts. A two-phonon state can interact with two different one-phonon states via the Fröhlich Hamiltonian, and a different phase is required for each of these because the interaction phase depends on $\mathbf{k}$. A compromise phase can be chosen, but as a result, the

effective strength of the interaction is reduced. In the trial wavefunction, I find that a phase can be chosen for the two-phonon states so that the total effective interaction with one-phonon parts is about 2/3 of the full interaction on average. Since the calculation applies to a weak coupling case, the contribution of two phonon states is relatively small, so it is not a bad approximation to ignore the phase entirely. The effect of this approximation is that the evaluated energy will be somewhat lower than the energy of the variational wavefunction. Note that for an electron confined in an analogous quasi-one dimensional quantum well, this approximation is not necessary. Using equation (35) to model the interaction allows an evaluation of the energy for the trial wavefunction. The ground state energy is shifted by $\Delta E_0 = -\alpha' \hbar\omega_{LO}$ where

$$\alpha' = -\frac{2}{\hbar\omega_{LO}} \sum_{\mathbf{q}} V_q e^{-q_\perp^2 L^2/4} g_{\mathbf{q}} - \sum_{\mathbf{q}} (1+(q_z/k_{LO})^2) |g_{\mathbf{q}}|^2 \quad (36)$$

Minimizing the energy with respect to $g_{\mathbf{q}}$ results in the expression

$$g_{\mathbf{q}} = -\frac{2m^*}{\hbar^2} \frac{V_q}{k_{LO}^2+q_z^2} e^{-q_\perp^2 L^2/4}. \quad (37)$$

The wave function

$$U_{LS}\Big[d\, c^\dagger_{k_x,k_z,0} |0\rangle + \sum_{\mathbf{q}} d_{\mathbf{q}} c^\dagger_{k_x-q_x,k_z-q_z,0} a^\dagger_{\mathbf{q}} |0\rangle\Big] \quad (38)$$

is used to describe the polaron at large wavevectors. Now the $g_{\mathbf{q}}$'s are fixed in the trial wavefunction, and the $d_{\mathbf{q}}$'s and d are used as variational parameters. This trial wavefunction can correctly describe polarons near the phonon energy because it allows the strong mixing of the zero phonon state with the $q_z=k_z$ one phonon states. If symmetry is used to set $d_{-q_x,-q_y,q_z} = d_{\mathbf{q}}$, then the energy minimization proceeds exactly as in the three dimensional case with the result (compare Ref. 4, eq. 25)

$$\frac{m^*\Delta E(k_z)}{\hbar^2} d = -k_z \sum_{\mathbf{q}} q_z g_{\mathbf{q}} d_{\mathbf{q}} \tag{39}$$

and

$$\tfrac{1}{2}\left(\frac{2m^*\Delta E(k_z)}{\hbar^2} + 2k_z q_z - k_{LO}^2 - q_z^2\right) d_{\mathbf{q}} = -k_z q_z g_{\mathbf{q}}\, d + q_z g_{\mathbf{q}} \sum_{\mathbf{q}'} q'_z g_{\mathbf{q}'}\, d_{\mathbf{q}'} \tag{40}$$

where

$$E(k_z) = \frac{\hbar^2 k_z^2}{2m^*} - \alpha' \hbar\omega_{LO} + \Delta E \tag{41}$$

is the energy of the polaron. Solving for the energy shift results in an implicit equation for the energy shift:

$$\Delta E(k_z) = 4\left(\frac{\Delta E(k_z)}{\frac{\hbar^2 k_z^2}{m^*} + 1}\right) \sum_{\mathbf{q}} \frac{\frac{\hbar^2}{2m^*} 2 q_z^2 k_z^2 (|g_{\mathbf{q}}|)^2}{\Delta E + \frac{\hbar^2}{2m^*}(2q_z k_z - k_{LO}^2 - q_z^2)}. \tag{42}$$

Converting the sum to an integral,

$$\Delta E = -\alpha k_{LO}^3 \left(\frac{\hbar^2}{\pi m^*}\right)\left[\frac{2m^*\Delta E}{\hbar^2} + 2k_z^2\right] \int_0^{\infty} q_\perp\, dq_\perp\, e^{-L^2 q_\perp^2/2}$$

$$\times \int_{-\infty}^{+\infty} \frac{q_z^2 dq_z}{(q_z^2 + q_\perp^2)(q_z^2 + k_{LO}^2)^2\,(q_z^2 - 2q_z k_z + k_{LO}^2 - \frac{2m^*}{\hbar^2}\Delta E)} \tag{43}$$

The q_z integral is done as a contour. The $q_\perp$ integral is done numerically, and the entire expression solved implicitly for ΔE. The results

of this calculation using parameters appropriate to GaAs ($\alpha \approx .07$)[17] are shown in figure 5 for the region near the phonon emission threshold, with energies measured relative to the interacting ground state energy. There is a significant energy lowering when k approaches k_{LO}, and the energy approaches the LO phonon energy only asymptotically as k gets large. This bending over of the dispersion curve increases with increasing magnetic field or electron confinement, essentially because phonons with larger transverse momentum can contribute to the energy lowering. Because we have included more than one phonon in our variational wavefunction, the energy pins one phonon energy above the shifted ground state energy rather than above the non-interacting ground state energy, regardless of how we treat the multi-phonon phase problem.

Appendix 2: Calculation of the Dependence of the Impact-Ionization Rate on Energy above Threshold in Magnetic Fields

Impact ionization involves two electrons in an impurity potential, and is thus complicated to treat theoretically. If the 2-electron subtleties of the problem are ignored, Fermi's Golden Rule can be applied in a straight-forward way to calculate the impact ionization rates. In this context, it is known as the Born Approximation. The main difficulty in this method is is that the usual plane wave solutions for the free electrons must be replaced by the unbound solutions of the Schrödinger equation which incorporates the impurity potential. This becomes very difficult if strong magnetic fields are also included, and has not been done. However, it is easy to show the dimensional effect of the magnetic field in the threshold region by using a few approximations.

The impact ionization rate of a neutral donor by an electron with wave vector **k** can be written, using Fermi's Golden Rule, as

$$r(\mathbf{k}) = \frac{2\pi}{\hbar} \sum_{\mathbf{k}_1,\mathbf{k}_2} \left| \langle \mathbf{k},0 | H_{e-e} | \mathbf{k}_1,\mathbf{k}_2 \rangle \right|^2 \delta\left(\frac{\hbar^2}{2m^*}(k^2 - k_1^2 - k_2^2) - E_D\right). \quad (44)$$

In this expression, $\mathbf{k}_1$ and $\mathbf{k}_2$ are the wave vectors of the two electrons resulting from the ionization, and
$\langle \mathbf{k}$
Error! enforces energy conservation, and is zero when the incident electron has insufficient kinetic energy to ionize the donor.

What is the dependence on of the ionization rate on k just above threshold? In this region, both $\mathbf{k}_1$ and $\mathbf{k}_2$ must be small and have a small and slowly varying effect on the magnitude of the electron-electron matrix element. Thus, the primary factor determining the variation of the impact ionization rate with k will be the number of available final states. When the sum is turned into an integral, the energy delta function results in a factor of the energy density of final states. For three dimensional electrons, the two-electron energy density of states is effectively that of a six dimensional

electron, and the energy density of states is thus proportional to the square of the energy. Thus, for incident energies very close to threshold, the impact ionization rate increases as the square of $\left(\frac{\hbar^2 k^2}{2m} - E_D\right)$.

In large magnetic fields, electrons become one-dimensional, in that their energy depends only on one wave vector component. The donor bound wavefunctions are also changed by the magnetic field, but the effect is mostly to increase the binding energy. For incident electrons very close to threshold, we can make the same argument as above, but because the final electron states are one dimensional, the two-electron energy density of states will be that of a two-dimensional electron, which is a step-function at zero energy. Thus, the onset of impact ionization should be much sharper in strong magnetic fields than in zero magnetic field.

Appendix 3: Other Work

Direct Radiative Substrate Heating for Molecular Beam Epitaxy[64].

I have been fortunate to work on an molecular beam epitaxy system which was unique in many ways when I began working with it. I was able to make a contribution to the characterization of this system, focussing on the substrate heating and mounting arrangement. Working with several others, I was able to demonstrate the significant advantages of direct radiative heating of wire mounted substrates over the older system of soldering wafers with indium. Conventional mounting techniques in molecular beam epitaxy using indium to solder GaAs substrates to molybdenum blocks result in a rough backside which is incompatible with integrated circuit processing. Using the radiative heating method, excellent temperature uniformity is achieved over a 3" wafer by a molybdenum holder ring design which minimizes contact with the substrate and holds the wafer against the back of the ring to eliminate shadowing of the substrate from the heater. Temperature measurement and control in this heater are done by radiative coupling to a shielded thermocouple which sits just behind the GaAs wafer. No coating of the wafers is necessary for temperature control. DLTS, photoluminescence, and mobility measurements show the clear superiority of GaAs layers grown using direct radiative substrate heating compared to conventional indium bonding.

In-situ Transmission Spectroscopy[65].

Again taking advantage of the unique configuration of our MBE system, I measured the infra-red light transmission through the GaAs substrates during growth. I was able to use this to determine substrate temperature and growth rates, solving a significant problem plaguing the indium-free holder.

The substrate temperature can be accurately determined by measuring the position of the band-gap absorption edge. The band gap of GaAs shifts about 50mV per 100°C in the usual temperature range of MBE growth, and has been well characterized previously. The position of the absorption edge can be measured to better than 5meV, so a temperature can be determined

with an accuracy of better than 10°C. The precision of the measurement is ±2°C. GaAs substrate temperatures as low as 450°C have been measured, and the technique is easily extendable to much lower temperatures. This technique was used to calibrate the thermocouple used to control the substrate heater during normal MBE growth.

The growth rates of $Al_xGa_{1-x}As$ and GaAs can be determined by measuring the Fabry-Perot interference fringes resulting from thin layers. For a single $Al_xGa_{1-x}As$ layer, the amplitude of the fringes observed as a function of time is a good measure of the index difference between the layer and the substrate. From published data about the GaAs index at high temperature, we can get the $Al_xGa_{1-x}As$ index, and thus an estimate of the Al mole fraction of the layer. The thickness of the layer can be determined by counting the fringes as the layer is grown. For a single layer of $Al_{0.3}Ga_{0.7}As$ on GaAs, fringes of magnitude 3.85%±0.62% at 1.468μm are observed. The optical thickness can be determined to within ±24nm. For multi-layer structures, the variations of the transmittance with wavelength become large, so that the optical thickness of both GaAs and AlAs can be extracted from a single wavelength scan. An accurate determination of the refractive indices of these materials at high temperatures could make this technique very important for the reproducible growth of $Al_xGa_{1-x}As$-GaAs heterostructures, because a high precision calibration can be done during each growth.

Polynomial Kinetic Energy Approximations for Indirect Heterostructures[89].

Electronic properties of complicated heterostructures incorporating both GaAs and AlAs are often impractical to calculate. I have proposed a new approximation to incorporate bandstructure into effective mass like wavefunctions which may be useful for calculating some of these properties.

The effective mass approximation, in which the band structure of a semiconductor is replaced by a simple parabolic dispersion relation for electrons, works surprisingly well for quantum calculations of electron eigenenergies and eigenstates in semiconductor heterostructures. It can be extended to systems with spatially varying effective mass by requiring wavefunction and particle flux continuity. However, for indirect heterostructures which include materials with electron bands of different sym-

metry, it fails to incorporate enough physics to give correct answers. An important example where effective mass calculations are inapplicable is the AlAs/GaAs system, in which the conduction band minima occur at the Γ and X points, respectively. The mixture of these two types of electrons in AlAs/GaAs superlattices has only been calculated using tight-binding or pseudopotential methods, which are difficult to apply to a wide range of heterostructures.

I have extended the spirit of effective mass calculations to a method applicable to indirect heterostructures. To do this, I write a Schrödinger equation in which the Hamiltonian is a n^{th} degree polynomial in the gradient operator, ∇. For any energy, there exist n (complex) plane wave solutions. For spatially varying band structures, we can write a probability conserving Schrödinger equation which has a flux operator consistent with the usual interpretation of plane wave group velocities. The requirements imposed by this Schrödinger equation on the wavefunction and its derivatives allow matching of the plane wave solutions across heterojunctions. I have applied this method to AlAs/GaAs double heterostructures, where interesting resonance and anti-resonance behaviors are seen. The computational speed of this method will allow complicated structures, including compositional grading and electric fields, to be modeled on microcomputers.

References

[1]K. von Klitzning, G. Dorda and M. Pepper, *Phys. Rev. Lett.* ***45***, 494 (1980).

[2]D. C. Tsui, H. L. Störmer and A. C. Gossard,*Phys. Rev. Lett.* ***48***, 1559 (1982).

[3] R. Dingle, H. L. Störmer, A. C. Gossard, and W. Wiegmann, *Appl. Phys. Lett.* ***33***, 665 (1978).

[4]T. Mimura, S. Hiyamizu, T. Fujii and K. Nanbu, *Jap. J. Appl. Phys.****19***, L225 (1980).

[5]W. J. Skocpol, L. D. Jackel, R. E. Howard, P. M. Mankiewich, D. M. Tennant, A. E. White and R. C. Dynes,*Surf. Sci.* ***170***, 1 (1986).

[6]R. A. Webb, A. B. Fowler and J. J. Wainer,*Surf. Sci.****142***, 1 (1984).

[7]K. S. Ralls, W. J. Skocpol, L. D. Jackel, R. E. Howard, L. A. Fetter, R. W. Epworth and D. M. Tennant, *Phys. Rev. Lett.* ***52***, 228 (1981).

[8]P. A. Lee and D. Stone, *Phys Rev. Lett.* ***55***, 1622 (1986).

[9]A. C. Gossard, J. H. English, P. M. Petroff, J. Cibert, G. J. Dolan and S. J. Pearton, *J. Cryst. Growth* ***81***, 101 (1987).

[10]M. A. Reed, R. T. Bate, K. Bradshaw, W. M. Duncan, W. R. Frensley, J. W. Lee and H. D. Shaw, *J. Vac. Sci. & Tech.* ***B4***, 358 (1986).

[11]J. Cibert, P. M. Petroff, G. Dolan, D. J. Werder, S. J. Pearton, A. C. Gossard and J. H. English, to be published in *Superlattices and Microstructures* (1987).

[12]K. Kash, A. Scherer, J. M. Worlock, H. G. Craighead and M. C. Tamargo, *Appl. Phys. Lett.* ***49***, 1043 (1986).

[13]W. Zawadski, *in Physics of Solids in Intense Magnetic Fields*, edited by E. D. Haidemenakis, (Plenum Press, New York, 1969), pp. 301-328.

[14] H. Sakaki, *Jpn. J. Appl. Phys.* ***19***, L735 (1980).

[15]H. Fröhlich, H. Pelzer and S. Zienan, *Phil. Mag* ***41***, 221 (1950).

[16]S. Das Sarma and B. A. Mason, *Ann. Phys.* ***163***, 78 (1985).

[17]G. Lindemann, R. Lassnig, W. Seidenbusch and E. Gornik, *Phys. Rev.* ***B 28***, 4693 (1983).

[18]B. K. Ridley, *J. Phys.* ***C 15***, 5899 (1982).

[19] F. A. Riddoch and B. K. Ridley, *Surf. Sci.* ***142***, 260 (1984).

[20]D. M. Larsen, *Phys. Rev.* ***144***, 697 (1966).

[21]J. Appel, *Rev. Mod. Phys.*, 193.

[22]G. Whitfield and R. Puff, *Phys. Rev.* ***139***, A338 (1965).

[23]F. M. Peeters, P. Warmenbol and J. T. Devreese, to be published in *Europhys. Lett.* (1987).

[24]D. M. Larsen, in *Polarons in Ionic Crystals andPolar Semiconductors*, edited by J. T. Devreese, (North Holland Publishing Co., Amsterdam, 1972), pp. 237-287.

[25]D. von der Linde, J. Kuhl and H. Klingenberg, *Phys. Rev. Lett.* ***44***, 1505 (1980).

[26]T. W. Hickmott, P. M. Solomon, F. F. Fang, Frank Stern, R. Fischer and H. Morkoç, *Phys. Rev. Lett.* ***52***, 2053 (1984).

[27]T. C. L. G. Sollner, W. D. Goodhue, P. E. Tannenwald, C. D. Parker and D. D. Peck, *Appl. Phys. Lett* ***43***, 588 (1983).

[28]L. V. Iogansen, *Sov. Phys. JETP* ***18***, 146 (1964).

[29]S. Luryi, *Appl. Phys. Lett.* ***47***, 490 (1985).

[30]N. Yokayama, K. Imamura, T. Ohshima, H. Nishi, S. Muto, K. Kondo and S. Hiyamizu, *Techical Digest of International Electron Device Meeting*, (unpublished, San Francisco, 1984).

[31]M. Heiblum, D. C. Thomas, C. M. Knoedler and M. I. Nathan, *Appl. Phys. Lett.* ***47***, 1105 (1985).

[32]K. Matsumoto, M. Ogura, T. Wada, N. Hashizume, T. Yao and Y. Hayashi, *Electr. Lett.* ***20***, 462 (1984).

[33]P. M. Solomon, C. M. Knoedler and S. L. Wright, *IEEE Trans. Electron. Dev.* ***ED-5***, 379 (1984).

[34]N. C. Cirillo, Jr., M. S. Schur, P. J. Vold, J. K. Abrokwah and O. N. Tufte, *I.E.E.E. Electr. Dev. Lett.* ***EDL-6***, 645 (1985).

[35]T. W. Hickmott, P. M. Solomon, R. Fischer and H. Morkoç, *J. Appl. Phys.* ***57***, 2844 (1985).

[36]T. W. Hickmott, P. M. Solomon, F. F. Fang, R. Fischer and H. Morkoç, in *Proc. of 17th International Conference on the Physics of Semiconductors*, edited by J. D. Chadi and W. A. Harrison, (Springer-Verlag, New York, 1985), p.417.

[37]Y. Yafet, R. W. Keyes and E. N. Adams, *J. Phys. Chem. Solids* ***1***, 137 (1956).

[38]C. B. Hanna, E. S. Hellman and R. B. Laughlin, *Phys. Rev.* ***B34***, 5475 (1986).

[39]J. P. LeBurton, *Phys. Rev.* ***B31***, 4080 (1985).

[40]L. Eaves, P. S. S. Guimaraes, F. W. Sheard, B. R. Snell, D. C. Taylor, G. A. Toombs and K. E. Singer, *J. Phys.* ***C 18***, L885 (1985).

[41]P. S. S. Guimaraes, D. C. Taylor, B. R. Snell, L. Eaves, K. E. Singer, G. Hill, M. A. Pate, G. A. Toombs and F. W. Sheard, *J. Phys.* ***C 18***, L605 (1985).

[42]J. Ihm, *Phys. Rev. Lett.* ***55***, 999 (1985).

[43]Pong-Fei Lu, D. C. Tsui, H. M. Cox, *Phys. Rev. Lett.* ***54***, 1563 (1985).

[44]J. R. Barker, *Physica* ***134B***, 22 (1985).

[45]E. S. Hellman, J. S. Harris, C. B. Hanna and R. B. Laughlin, *Physica* ***134B***, 41 (1985).

[46]E. S. Hellman and J. S. Harris, Jr., *Phys. Rev.* ***B33***, 8284 (1986).

[47]H. J. Stocker, H. Levinstein and C. R. Stannard, Jr., *Phys. Rev.* ***150***, 613 (1966).

[48]Y. Katayama and K. F. Komatsubara, *Phys. Rev. Lett.* ***19***, 1421 (1967).

[49]C. B. Hanna and R. B. Laughlin, *Phys. Rev. Lett.* ***56***, 2547 (1986).

[50]B. C. Cavenett, *Phys. Rev.* ***B5***, 3049 (1972).

[51]I. O. Kulik and R. I. Shekhter, *Phys. Lett.* ***98A***, 132 (1983).

[52]Pong-Fei Lu, D. C. Tsui, H. M. Cox, to be published in*Phys. Rev.* (1987).

[53]L. Eaves, P. S. S. Guimaraes, B. R. Snell, D. C. Taylor and K. E. Singer, *Phys. Rev. Lett.* ***55***, 262 (1985).

[54]D. C. Taylor, P.S. S> Guimaraes, B. R. Snell, L. Eaves, F. W. Sheard, G. A. Toombs, K. Singer, *Physica* ***134B***, 12 (1985).

[55]L. Eaves, B. R. Snell, D. K. Maude, P. S. S. Guimaraes, D. C. Taylor, F. W. Sheard, G. A. Toombs, J. C. Portal, L. Dmowski, P. Claxton, G. Hill, M. A. Pate and S. J. Bass,in *Proc. 18th International Conference on the Physics of Semiconductors*, edited by O. Engström, (World Scientific, Singapore, 1987), 1615.

[56]T. W. Hickmott, *Phys. Rev.* ***B32***, 6531 (1985).

[57]L. Eaves, *Bull. Am. Phys. Soc.* ***32***, 886 (1987).

[58]P. M. Campbell, J. Comas, R. J. Wagner and J. E. Furneaux, *Bull. Am. Phys. Soc.* ***32***, 886, (1987).

[59]R. A. Reynolds, *Sol. St. Electr.* ***11***, 385 (1968).

[60]T. Wang, J. P. Leburton, K. Hess and D. Bailey, *Phys. Rev.* ***B33***, 2906 (1986).

[61]C. Hanna and R. B. Laughlin, *Bull. Am. Phys. Soc.* ***30***, 631 (1985).

[62]E. C. Larkins, E. S. Hellman, D. G. Schlom, J. S. Harris Jr., M. H. Kim, G. E. Stillman, *Appl. Phys. Lett.* ***49***, 391 (1986).

[63]G. E. Stillman, *private communication*.

[64]E. S. Hellman, P. M. Pitner, A. Harwit, D. Liu, G.W. Yoffe, J. S. Harris, Jr., B. Caffee and T. Hierl, *J. Vac. Sci. & Tech.* ***B4***, 574 (1985).

[65]E. S. Hellman and J. S. Harris, Jr., *J. Cryst. Growth* ***81***, 38 (1987).

[66]A. Chandra, C. E. C. Wood, D. W. Woodard and L. F. Eastman, *Sol. St. Electr.* ***22***, 645 (1979).

[67]C. M. Wolfe, G. E. Stillman and W. T. Lindley, *J. Appl. Phys.* ***41***, 3088 (1970).

[68]C. Kocot and C. A. Stolte, *I.E.E.E. Trans. Electr. Dev.* ***ED-29***, 1059 (1982).

[69]E. M. Conwell, "High Field Transport in Semiconductors", in*Solid State Phys.****Suppl. 9***, (Academic Press, New York, 1967).

[70]J. G. Ruch and W. Fawcett, *J. Appl. Phys.* ***41***, 3843 (1970).

[71]C. M. Wolfe, G. E. Stillman and J. O. Dimmock, *J. Appl. Phys.* ***41***, 504 (1970).

[72]A. L. McWhorter and R. H. Rediker, *Proc. IRE* ***47***, 1207 (1959).

[73]D. J. Oliver, *Phys. Rev.* ***127***, 1045 (1962).

[74]T. O. Poehler, *Phys. Rev.* ***B4***, 1223 (1971).

[75]G. E. Stillman, C. M. Wolfe, I Melngailis, C. D. Parker, P. E. Tannenwald and J. O. Dimmock, *Appl. Phys. Lett.* ***13***, 83 (1968).

[76]L. Eaves and J. C. Portal, *J. Phys.* ***C 12***, 2809 (1979).

[77]R. J. Nicholas and R. A. Stradling, *J. Phys.* ***C 9***, 1253, (1976).

[78]V. N. Zverev and D. V. Shovkun, *Sov. Phys. JETP* ***60***, 1003 (1984).

[79]R. L. Peterson,*Semiconductors and Semimetals* ***10***, 221 (1975).

[80]L. Eaves, R. A. Stradling, S. Askenazy, R. Barbaste, G. Carrère, J. Leontin, J. C. Portal and J. P. Ulmet, *J. Phys.* ***C 7***, 1999 (1974).

[81]D. M. Larsen, *J. Phys. Chem. Solids* ***29***, 271 (1968).

[82]M. E. Cohen and P. T. Landsberg, *Phys. Rev.* ***154***, 683 (1967).

[83]J. R. Hayes, A. J. F. Levi and W. Wiegmann, *Phys. Rev. Lett.* ***54***, 1570 (1985).

[84]J. Franck and G. Hertz, *Deutsch. Phys. Gesell.* **16**, 457 (1914).

[85]D. M. Larsen, *Phys. Rev.* ***135***, A419 (1964).

[86]D. M. Larsen, *Phys. Rev.* ***142***, 428 (1966).

[87]E. Haga, *Prog. Theoret. Phys. (Kyoto)* ***13***, 555 (1955).

[88]F. Low, T. D. Lee and D. Pines, *Phys. Rev.* ***90***, 297 (1953).

[89]E. S. Hellman and J. S. Harris, Jr., to be published in *Superlattices and Microstructures,* (1987).